

DTIC FILE COPY

①

AD-A199 382

NUSC Technical Document 8055
30 September 1987

The Ships Below-Decks Electromagnetic Compatibility (EMC) Program

A Compilation of Papers
Presented at the
1987 IEEE International Symposium on EMC

Submarine Electromagnetic Systems Department



DTIC
ELECTE
SEP 19 1988
S H D

Naval Underwater Systems Center
Newport, Rhode Island / New London, Connecticut

Approved for public release; distribution unlimited.

88 9 19 072


Preface

This document was prepared under Project No. A51000, The Ships Below-Decks EMC Program, Principal Investigator D.S. Dixon (Code 3431). The Sponsoring Activity is the Office of The Chief of Naval Research/Office of Naval Technology; Submarine Technology Program Element Manager G. Remmers (Code 233). The Submarine Technology Block Program Manager is L. Cathers (Code 012.4) of the David W. Taylor Naval Ship Research and Development Center.

Important contributions required to conduct the work were made by G & H Technology, Inc., Moore School of Electrical Engineering, University of Pennsylvania, and Western New England College under contract to the Naval Underwater Systems Center.

The authors wish to acknowledge the contribution of John Miller, EMC consultant for G & H Technology, Inc., who provided the triaxial fixture test method and measurement data for the EMI performance evaluation of the shield ground adapters.

Reviewed and Approved:



D.F. Dence

Submarine Electromagnetic Systems Department

REPORT DOCUMENTATION PAGE

1a. REPORT SECURITY CLASSIFICATION UNCLASSIFIED		1b. RESTRICTIVE MARKINGS	
2a. SECURITY CLASSIFICATION AUTHORITY		3. DISTRIBUTION / AVAILABILITY OF REPORT Approved for public release; distribution unlimited.	
2b. DECLASSIFICATION / DOWNGRADING SCHEDULE		5. MONITORING ORGANIZATION REPORT NUMBER(S)	
4. PERFORMING ORGANIZATION REPORT NUMBER(S) TD 8055		7a. NAME OF MONITORING ORGANIZATION	
6a. NAME OF PERFORMING ORGANIZATION Naval Underwater Systems Center	6b. OFFICE SYMBOL (If applicable)	7b. ADDRESS (City, State, and ZIP Code)	
6c. ADDRESS (City, State, and ZIP Code) New London Laboratory New London, CT 06320-5594		9. PROCUREMENT INSTRUMENT IDENTIFICATION NUMBER	
8a. NAME OF FUNDING / SPONSORING ORGANIZATION OCNR/ONT	8b. OFFICE SYMBOL (If applicable) Code 233	10. SOURCE OF FUNDING NUMBERS	
8c. ADDRESS (City, State, and ZIP Code) Washington, DC 20362		PROGRAM ELEMENT NO. 62323N	PROJECT NO. RB23C55
11. TITLE (Include Security Classification) The Ships Below-Decks Electromagnetic Compatibility (EMC) Program		TASK NO.	WORK UNIT ACCESSION NO.
12. PERSONAL AUTHOR(S) Dixon, David S., Compiler			
13a. TYPE OF REPORT Progress	13b. TIME COVERED FROM SEP 86 TO OCT 87	14. DATE OF REPORT (Year, Month, Day) 1987 SEP 30	15. PAGE COUNT 47
16. SUPPLEMENTARY NOTATION A Compilation of Papers Presented at the 1987 IEEE International Symposium on EMC			
17. COSATI CODES		18. SUBJECT TERMS (Continue on reverse if necessary and identify by block number)	
FIELD	GROUP	SUB-GROUP	EMC Composite Connectors Conducted Emission Models
17	04		EMI Crosstalk Switching Power Supplies
11	04		EMI/EMP Protection Shield Ground Adapters
19. ABSTRACT (Continue on reverse if necessary and identify by block number)			
<p>1. "An Evaluation of the Long Term EMI Performance of Several Shield Ground Adapters" (David S. Dixon, Stanley I. Sherman, Michael Van Brunt) proved that, if the degradation caused by the kickpipe threads can be reduced, a new technology shield ground adapter (SGA), with a solid shield contactor, will ensure the highest long term SGA performance, thereby reducing below-decks electromagnetic (EM) levels caused by EMI/EMP cable currents.</p> <p>2. "A Full Performance Composite Connector with Long Term EMI Shielding Properties" (James V. Masi, David S. Dixon, Maurice Avoux) discusses development of a full MIL-SPEC connector made from composite materials that was designed to satisfy a full range of EM, chemical, and mechanical properties. A mathematical model was developed to give a basis for predicting some of the EM properties of a composite material.</p>			
20. DISTRIBUTION / AVAILABILITY OF ABSTRACT <input checked="" type="checkbox"/> UNCLASSIFIED/UNLIMITED <input type="checkbox"/> SAME AS RPT. <input type="checkbox"/> OTC USERS		21. ABSTRACT SECURITY CLASSIFICATION UNCLASSIFIED	
22a. NAME OF RESPONSIBLE INDIVIDUAL David S. Dixon		22b. TELEPHONE (Include Area Code) (203) 440-4453	22c. OFFICE SYMBOL 3431

19. (Cont'd)

3. "Conducted Emission Models for Switching Power Supplies" (Anthony B. Bruno) discusses computer modeling of the effect of nonlinear loads on military power distribution systems, incorporating both low (CE01) and high (CE03) frequency emissions. The results agree well with actual shipboard measurements.

4. "Crosstalk in Coaxial Transmission Systems" (Steven J. Peters, Ralph M. Showers) examines the crosstalk between two parallel braided shield coaxial cables. At high frequencies, the integral equation approach was much more accurate at predicting the crosstalk than transmission line theory.

5. "Development of Models for the Shield Ground Adapter" (Ralph M. Showers, Steven J. Peters) presents a theoretical model for an adapter to be used for grounding the external shield of a cable to a plate it penetrates. The model shows good agreement with measurements up to at least 500 MHz.



Accession For	
NTIS GEAR	<input checked="" type="checkbox"/>
ERIC Doc	<input type="checkbox"/>
Unannounced	<input type="checkbox"/>
Distribution/	
Availability Codes	
Dist	Special
A-1	

TABLE OF CONTENTS

1. AN EVALUATION OF THE LONG TERM EMI PERFORMANCE OF SEVERAL SHIELD GROUND ADAPTERS	1-1
Abstract	1-1
Background	1-1
Environmentally Sealed SGAs	1-1
Need for Long Term SGA Performance Evaluation	1-2
Performance Validation of Existing and New Technology SGAs	1-2
Transfer Impedance (Zt) Testing with Shielded Room	1-2
Triaxial Test Fixture Transfer Impedance Measurement Method ...	1-3
Comparison of Zt Test Data with Predicted (EMI Model) Performance	1-3
Evaluation of the DC Performance of Existing and New Technology SGAs	1-5
Long Term Performance Validation of Existing and New Technology SGAs	1-6
Long Term AC Performance Evaluation of Existing and New Technology SGAs	1-8
Improved Solid Cable Shield Contactor: New Technology SGA Developed	1-9
Conclusions	1-10
Recommendations	1-10
Acknowledgments	1-11
References	1-11
2. DEVELOPMENT OF A FULL PERFORMANCE COMPOSITE CONNECTOR WITH LONG TERM EMI SHIELDING PROPERTIES	2-1
Abstract	2-1
Background	2-1
Initial Resin/Filler Selection and Evaluation	2-1
A Theoretical Model to Predict the Electromagnetic Properties of Composite Materials	2-2
DC Case	2-3
AC Case	2-4
Results	2-4
Conclusions	2-5
Acknowledgments	2-5
References	2-5
3. CONDUCTED EMISSION MODELS FOR SWITCHING POWER SUPPLIES	3-1
Abstract	3-1
Introduction	3-1
Computer Model	3-2
The CE01 Model	3-2
CE03 Emission Model	3-5
Sample Power Supply Runs	3-6
Conclusions	3-8
Acknowledgments	3-8
References	3-8

(Cont'd) TABLE OF CONTENTS

4. CROSSTALK IN COAXIAL TRANSMISSION SYSTEMS	4-1
Abstract	4-1
Introduction	4-1
Formulation of the Problem	4-1
Transmission Line Solution for the External Shield Currents ...	4-1
Integral Equation Solution for the External Shield Currents ...	4-2
Relationship Between Transmission Line Theory and the Integral	
Equation Approach	4-4
Internally Induced Voltages	4-4
Experimental Procedure	4-5
Conclusions	4-5
Acknowledgments	4-6
References	4-6
5. DEVELOPMENT OF MODELS FOR THE SHIELD GROUND ADAPTER	5-1
Abstract	5-1
Introduction	5-1
The Exposed Cable	5-1
Measures of Effectiveness	5-1
Model Impedance Characteristics	5-2
Equivalent Circuit	5-2
The Input Line	5-3
Output Line	5-3
Calculation of Shielding Effectiveness	5-3
Mutual Inductance	5-4
Correlation with Experimental Data	5-5
Refining the Equivalent Circuit	5-5
Conclusions	5-6
Acknowledgments	5-7
References	5-7

An Evaluation of the Long Term EMI Performance of Several Shield Ground Adapters

DAVID S. DIXON, MEMBER, IEEE, and STANLEY I. SHERMAN, MEMBER, IEEE

Naval Underwater Systems Center
New London Laboratory (NUSC/NLL)
New London, CT 06320

and

MICHAEL VAN BRUNT
G & H Technology, Inc.
750 W. Ventura Blvd.
Camarillo, CA 93010

ABSTRACT

A shield ground adapter (SGA) is a device utilized to establish a 360° low impedance electrical connection between a cable's shield and the ground structure through which the cable passes. This low impedance connection is designed to reduce and/or eliminate EMI and/or EMP problems by shunting high level currents into the systems' ground plane. This paper will discuss the measured EMI performance characteristics of an existing (spring) technology SGA and a new technology SGA that utilizes a recently developed smart-soldering technique and an improved cable shield-to-SGA connection method. Over one year ago, one new construction model of each SGA was installed on the deck of a U.S. naval ship. This paper will discuss the a.c. and d.c. EMI measurements that were conducted on the SGAs. The measurements were conducted both before the installation and one year later, after being exposed to 12 months of a harsh marine environment.

BACKGROUND

A metallic boundary is typically established by EMI and EMP personnel to protect electronic equipment from high level electromagnetic fields. These fields can be created in peacetime by lightning and nearby communication transmitters or in times of conflict by an Electromagnetic Pulse (EMP). In certain instances it is necessary to have shielded signal cables transition this metallic boundary. It is estimated that over 80 dB of attenuation is required at such interfaces to reduce the hundreds of amperes of current that could be flowing on cable shields. One method of preventing electronic system damage is to shunt these currents into the system ground plane at the point where these cables pass through the grounded metallic boundary. This can be accomplished by employing devices referred to as Shield Ground Adapters (SGAs). This type of protection may be required at the topside-to-below decks interface of a ship or the external-to-internal interface of a building, or the compartment-to-compartment interface between isolated below-decks spaces.

Early EMC work on FFG-7 Class platforms indicated that EMI energy was being coupled into below-decks areas by currents flowing on cable shields. These currents were producing below-deck environmental levels exceeding the "normal" environmental levels assumed by MIL-STD-461 for electronic equipments. Initial efforts to reduce these below-deck field levels by grounding cable shields produced significant reduction of below-deck field strengths. These reductions came in spite of the temporary and unsophisticated nature of various grounding techniques initially utilized to connect the cable shield to the ship's hull. Military specifications [1] for electronic equipment now recommend the use of SGAs to reduce cable shield currents.

ENVIRONMENTALLY SEALED SGAsEARLY SGAs

Figure 1 illustrates the evolution of cable shield grounding devices. The earliest environmentally sealed SGAs utilized ballpoint pen style springs that were connected end-to-end around the signal cable's shield. These springs were then compressed against the signal cable's shield to shunt EMI currents into the system or platform ground plane. This type of SGA utilizes a spring member that encircles the shield of a typical R.G. cable. This spring member is then mechanically compressed when assembled. The operational performance of this grounding device is directly related to the contact force between the shield and the spring member. The essence of this type of device is maintaining a certain amount of contact force that yields a certain level of transfer impedance (Z_t). There exists several modes that can and do degrade the performance of these devices. The level of performance (Z_t) is directly related to the contact force between the shield and the spring member. Typical shipboard cables such as R.G. 214 have a dielectric inner, which can cold flow due to excessive compressive force of the grounding spring. If this cold flow phenomenon takes place, the contact force between cable shield and spring contact will change, possibly affecting the performance of the signal being transmitted along the cable.

It was suspected that the EMI/EMP performance of this compression type of SGA would deteriorate with both time and environmental influences due to its spring-to-shield pressure method of achieving the necessary 360° contact between the cable shield and the system (or shipboard) ground plane. The suspected problems with this type of pressure sensitive shield contact became the basis for the Navy investing in research and development into the grounding of shielded cables and conduit.

Reference 2 delineated the short-term performance loss that was measured for an existing spring compression technology SGA. The SGA's performance deterioration after 6 hours ranged from 8 to 22 dB, over the frequency range from 1 MHz to 40 MHz. This performance loss increased with time such that after 24 hours the performance loss ranged from 13 to 34 dB.

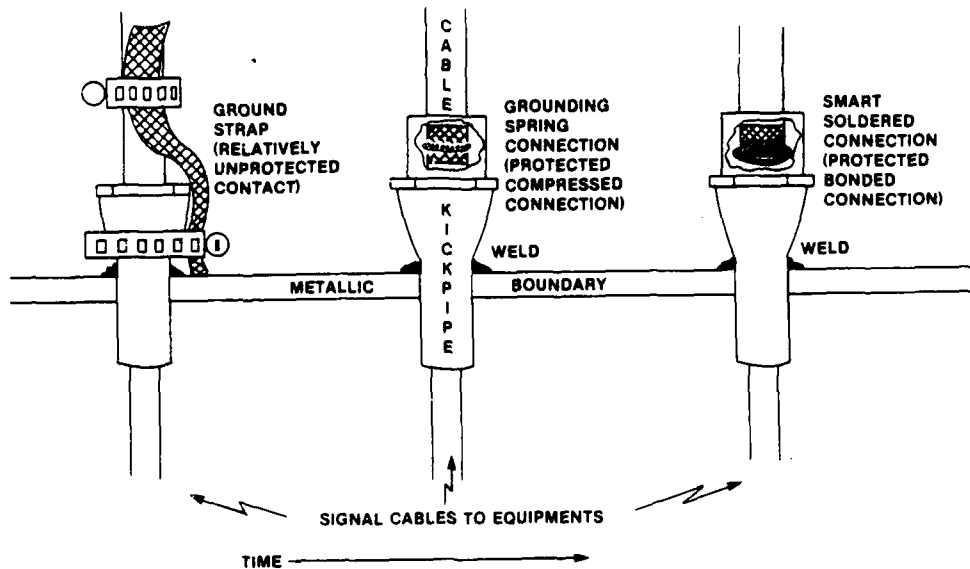


Figure 1: Cable Shield Ground Evolution

NEW TECHNOLOGY SGA

In a combined effort between the Naval Underwater Systems Center (NUSC), G & H Technology Inc. (G & H), and the University of Pennsylvania (UPENN), an improved SGA has been developed that will maintain a higher level of performance over the lifetime of the SGA, even after being exposed to hostile marine environments. This improvement is due to the utilization of a new method of bonding the cable grounding contact to the cable shield and to the development of an SGA that will connect the grounding contact to the system/platform ground. This new grounding contact is attached to the cable shield by soldering it to the shield utilizing a METCAL developed self-regulating temperature source (SR/TS) with their solder strap connection system [3]. Utilizing this technique, soldering temperatures are accurately maintained at levels high enough to provide an excellent solder bond between the grounding contact and the cable shield, but low enough to prevent any change in the cable's transmission characteristics. A paper by Van Brunt [4] discussed the mechanical design aspects of this new technology SGA.

NEED FOR LONG-TERM SGA PERFORMANCE EVALUATION

In order to evaluate the long-term performance of both existing and new technology SGAs, a new construction model (solid version vice retrofit split decks interface of an FFG-7 Class Frigate. This would expose both devices to the hostile topside environment of a surface ship for over one year. Pre and post installation d.c. and a.c. Z_t measurements were conducted on each SGA at both NUSC and G & H. In addition, shipboard d.c. measurements were also conducted on each SGA after six months of exposure to the topside environment.

PERFORMANCE VALIDATION OF EXISTING & NEW TECHNOLOGY SGAs

METHODS OF A.C. PERFORMANCE EVALUATION

Two methods of evaluating SGA performance have been utilized during this SGA development effort:

1. The first test method used to evaluate the SGA performance utilized a shielded room to isolate the SGAs input from its output. This procedure measured input current $I(in)$ and the SGA output voltage between the cable shield and the ground plane $V(out)$. This produced a $V(out)/I(in)$ ratio or a SGA transfer impedance, Z_t , which was proportional to the SGA's performance.

2. The second test method utilized a triaxial test fixture where an internally mounted incorel current probe measured $I(in)$, and an internal connection between the cable shield and the system ground provided $V(out)$.

TRANSFER IMPEDANCE (Z_t) TESTING WITH SHIELDED ROOM

As shown in figure 2, a shielded room at NUSC was utilized to conduct transfer impedance (Z_t) measurements at frequencies up to 30 MHz. The shielded room was utilized to electromagnetically isolate the SGA input from its output. A high power wideband amplifier was used to drive approximately 4 amperes of V.L.F. and H.F. currents down the coaxial cable shield. The SGA output-side of the cable shield was terminated inside the shielded room by the 50 Ohm input circuitry of the spectrum analyzer. Because of the very low values of shield-to-ground output voltage $V(out)$ being measured, careful attention was given to the test apparatus grounding configuration. To improve measurement sensitivity, all the high level "source" equipment were placed outside of the shielded room, and the low level output measurement equipment were placed inside the shielded room.

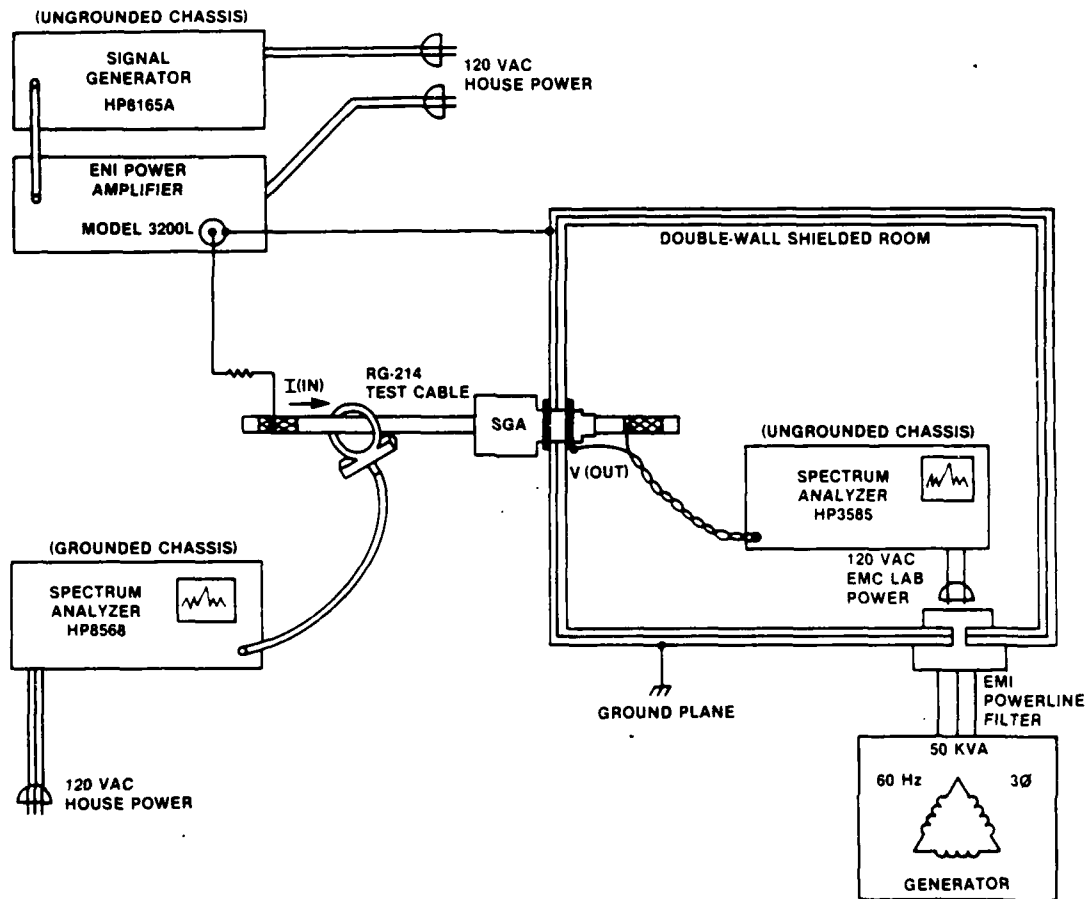


Figure 2: NUSC Transfer Impedance (Z_t) Measurement Procedure Utilizing a Shielded Room

The SGA output shield-to-ground voltage being measured can be modeled as a voltage source with a series resistance equal to the contact resistance between the cable shield and the SGA. At most, this resistance is on the order of a few milli-Ohms. For testing purposes, this voltage is a good parameter to measure because it is inherently immune to all the cable variables associated with using a dual current probe measurement method. This measurement of performance is defined as $V(out)/I(in)$, and it can be seen that it has the units of impedance (Z_t). This unit of performance is independent of the SGA installation, because the shield impedance at the SGA output will always be significantly more than the defined source impedance of the measured voltage; therefore, the configuration of the output side of the cable will have no significant effect on the $V(out)$ measurement. Thus this $V(out)/I(in)$ ratio provides a transfer impedance (Z_t) value that is dependent on the effectiveness of the SGA shunt device and independent of output cable configuration.

TRIAxIAL TEST FIXTURE TRANSFER IMPEDANCE MEASUREMENT METHOD

A test fixture was constructed at G & H that would measure the SGA performance over an extended frequency range from 10 MHz to 200 MHz. The fixture

shown in figure 3 was constructed to accommodate the termination of a shielded cable whose diameter was as great as that of a R.G. 319 rigid coax (2.5 inches). The fixture is a modified version of a MIL-SPEC triaxial fixture. It is basically operated in a shorted coax configuration with the input fed on one side of the short and the output taken on the other. The input is coaxial, externally loaded, and internally shorted, and an incoel current sensor is placed at the shorted end. The output section is coaxial, internally shorted, and externally loaded. The fixture resembles a stubb triax with the exception of the added current sensor. The sensitivity of this system is approximately 5 nano-Ohms.

COMPARISON OF Z_t TEST DATA WITH PREDICTED EMI MODEL PERFORMANCE

For frequencies below 30 MHz, comparisons of transfer impedance test data were made between the triaxial measurement procedure and the shielded room measurement procedure. As shown in figure 4 this comparison of test data from the same new construction, fingered shield contactor SGA, yielded SGA transfer impedance (Z_t) values that were within 4 dB of each other. This closeness in data occurred in spite of the fact that the SGA was tested using

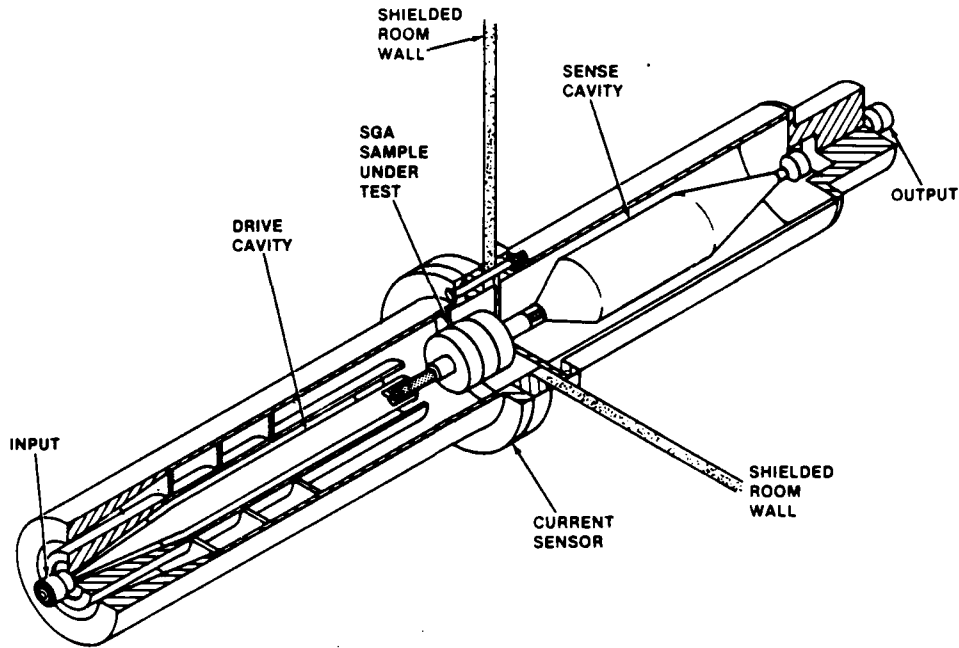


Figure 3: G&H Technology Transfer Impedance (Z_t) Measurement Test Fixture

completely different: (1) measurement equipment, (2) personnel, (3) shielded rooms; (4) test procedures, and the data was measured almost two weeks apart on the East and West Coasts. Considering all of the variables involved with each set of Z_t measurements, the closeness of the data demonstrated a high confidence level in the accuracy of the a.c. Z_t measurements.

In addition to the measured data, the program required that an EMI model be developed to predict the performance of the new technology SGA. If measured and predicted data were reasonably close (within 10 dB) then confidence in the measured

performance would be very high. Also, and perhaps most important, the model would allow potential SGA improvements to be evaluated on the computer, thereby saving time and money normally expended by conducting SGA performance testing. The mathematical SGA EMI model developed by Dr. Ralph Showers and Mr. Steve Peters [5] also falls within 4 dB of the NUSC and G & H test data illustrated in figure 4. The model data and the measured data is for an early version of the new technology SGA. This SGA had a fingered shield contactor rather than the solid contactor ultimately used to optimize SGA performance.

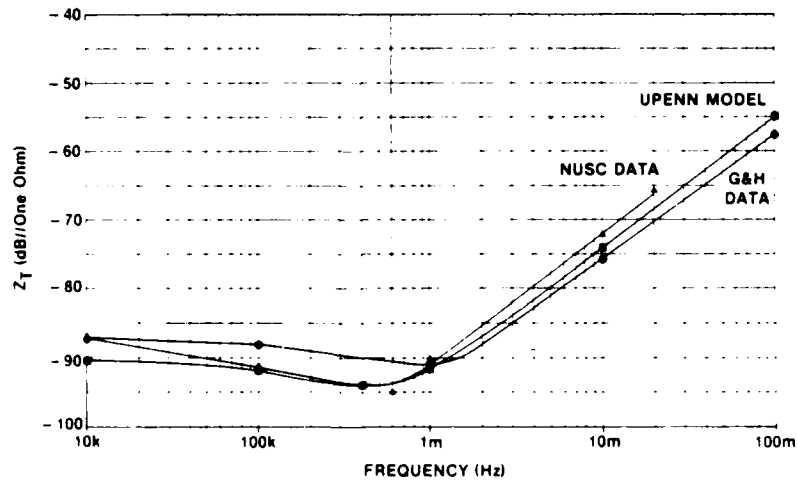


Figure 4: Comparison of NUSC (Shielded Room) and G&H (Triaxial Fixture) Measurement Systems Test Data with the UPENN EMI Model

EVALUATION OF THE D.C. PERFORMANCE OF EXISTING AND NEW TECHNOLOGY SGAs

D.C. TEST CONFIGURATIONS

It was demonstrated in the EMC laboratory at NUSC/NL that a.c. values of Z_t were too small to be measured in the shipboard environment due to other nearby hull penetrations that caused EMI coupling between topside and below-deck areas. This coupling necessitated that all a.c. SGA performance measurements be made in the laboratory. However, it was possible to make shipboard measurements of d.c. Z_t . Even in the electromagnetically noisy shipboard environment, whenever a large d.c. current, $I(in)$, was injected on the input side of the cable shield, a voltage, $V(out)$, could be measured on the SGA output side of the cable shield. This measurement was necessary to verify the initial and periodic integrity of the shield to ground contact. As shown in figure 5, d.c. resistance measurements were made between test points A through E by driving 4 amperes of d.c. current down the cable shield and measuring the d.c. voltage between test points A through E. The physical differences between the two SGAs installed on the ship and the exact location of each test point is illustrated in figure 6.

NEED FOR KICKPIPE EXTENSION

The SGAs are designed to screw into a standard kickpipe (an environmentally sealed cable penetration through the deck) that is welded to the deck, and a method was needed to measure the electrical

performance of the SGA-to-kickpipe thread interface. To accomplish this goal, a kickpipe extension was made from the same aluminum alloy as the kickpipe. The interface between the SGAs and the extensions had the same electrical, mechanical, and electro-chemical properties that the SGA-to-kickpipe interface would have had. Using the extension allowed removal of the SGA-to-kickpipe extension interface from the ship without disturbing the cable shield-to-SGA connection integrity, thereby permitting a repeat of the pre-environmental EMI testing in the electromagnetically quiet laboratory environments of NUSC and G & H.

D.C. PERFORMANCE AFTER FIVE MONTHS OF SHIPBOARD EXPOSURE

Measurements of voltage between test points A & D (see figure 5) for both an existing spring compression style SGA and a first generation shielded contactor style SGA, indicated the following:

1. Initial pre-installation d.c. values of Z_t for both devices were very similar,
2. After five months of exposure to the shipboard environment:
 - a. the d.c. Z_t for the 1st generation smart-soldered style SGA increased (degraded) by 2.1 dB, (3.7 to 4.7 mV)/4A.

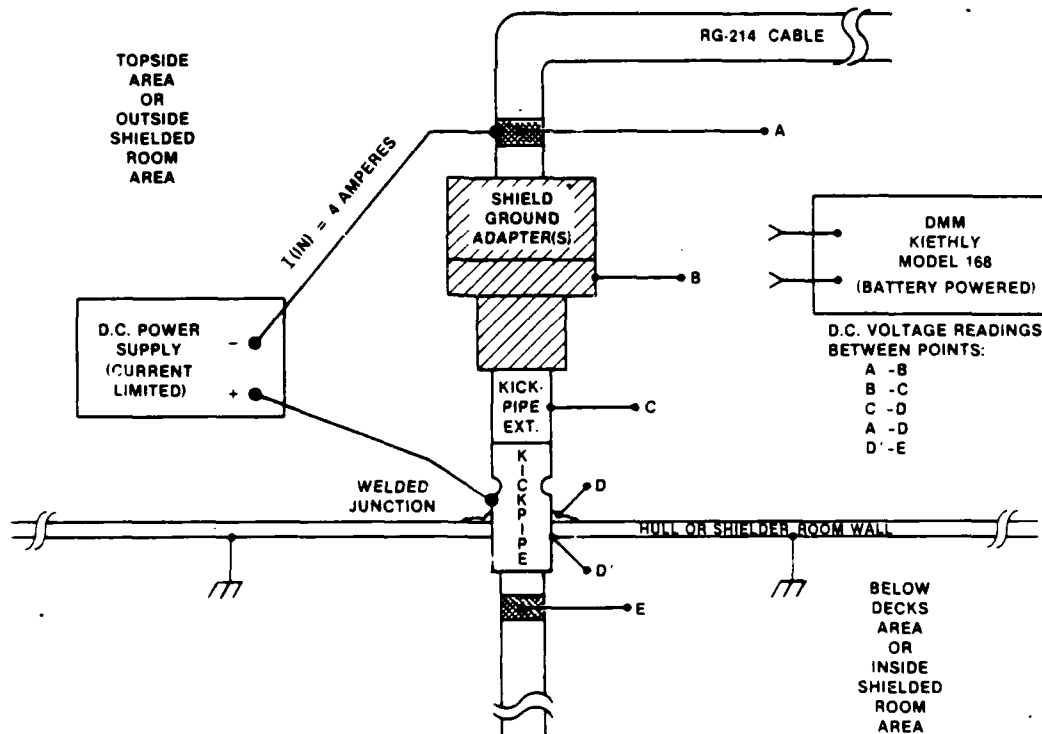


Figure 5: D.C. Transfer Impedance Measurement Configuration (Shipboard Measurement)

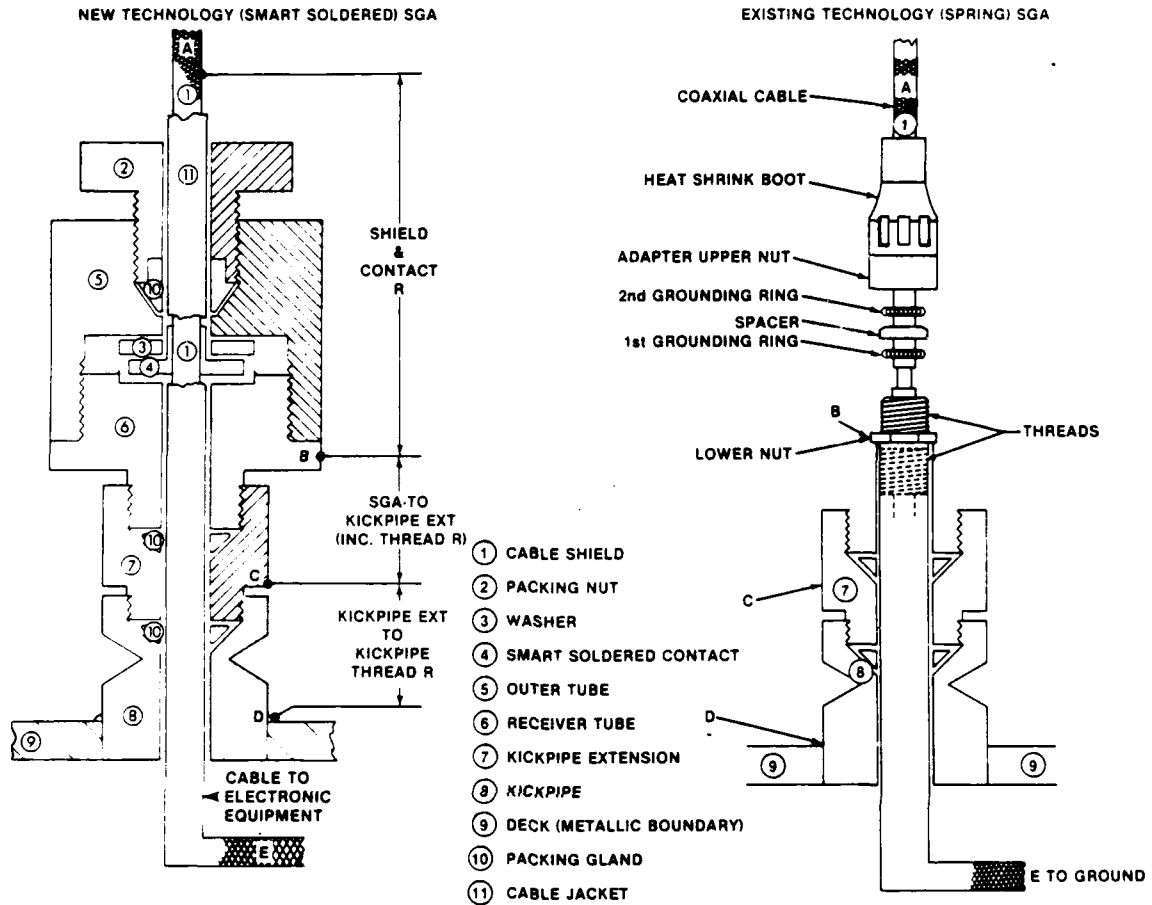


Figure 6: Physical Models of the New Technology (Smart Soldered) and Existing Technology (Spring-compression) Shield Ground Adapters

- b. the d.c. Z_t for the spring compression style SGA increased (degraded) by 17.1 dB, (5.4 to 38.8 mV)/4A.
- 3. Even at that early time, preliminary analysis indicated that threaded interfaces, such as the SGA-to-kickpipe extension interface, might be very crucial in determining long term SGA performance.

LONG TERM PERFORMANCE VALIDATION OF EXISTING AND NEW TECHNOLOGY SGAs

EVALUATIONS OF SGAs AFTER ONE YEAR OF SHIPBOARD EXPOSURE

Utilization of the kickpipe extension discussed above was to have permitted the removal of the SGAs from the ship without disturbing the cable shield-to-SGA connection, thereby permitting a repeat of the pre-installation a.c. EMI testing that had been conducted in the quiet laboratory environments. Inconsistent post-installation laboratory a.c. and

d.c. Z_t values indicate that this goal may not have been achieved i.e., apparently, movement of the SGAs during removal from the ship, during testing at NUSC, or during shipment to the West Coast for G & H testing caused physical stress/vibration within the SGA that resulted in inconsistent Z_t data.

SHIPBOARD MEASUREMENTS, D.C. PERFORMANCE-VS-TIME

The d.c. measurements conducted on the ship were a good barometer of SGA performance over time. As shown by other laboratory measurements, the low frequency a.c. and the d.c. data points are almost exact. In fact, it was this difference in d.c. data points (d.c. ship & d.c. lab & a.c. lab) that alerted the measurement team that movement of the SGA was causing changes in the SGA's performance.

Figure 6 illustrates the d.c. performance degradation-vs-time of the existing (spring) technology SGA over the 12 month period of time it was installed on the ship. The d.c. measurement results plotted in figures 7 & 3 were measured at the

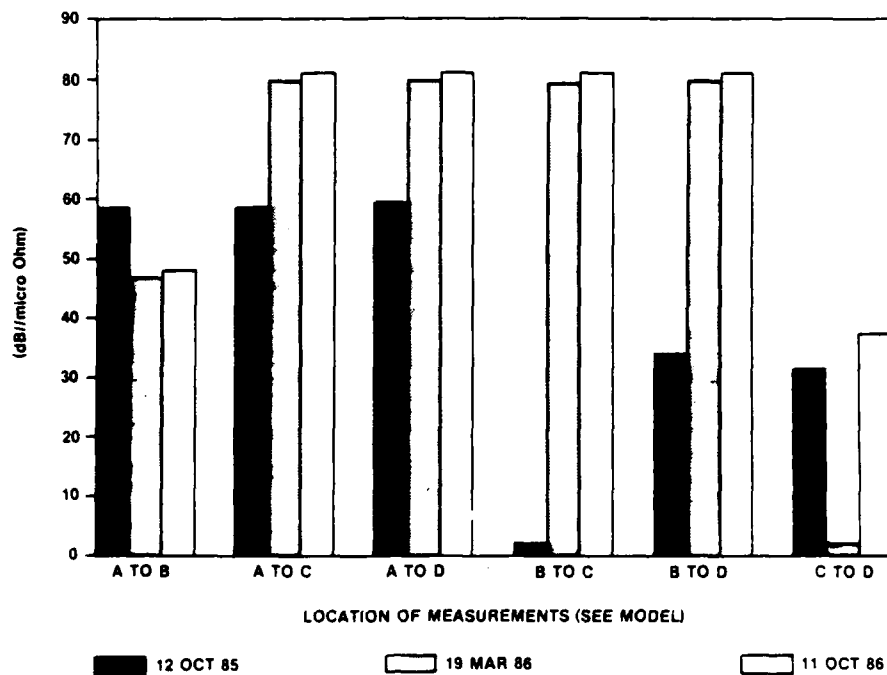


Figure 7: Shipboard D.C. Measurements-vs-Time for the Existing (Spring-Compression) Technology SGA

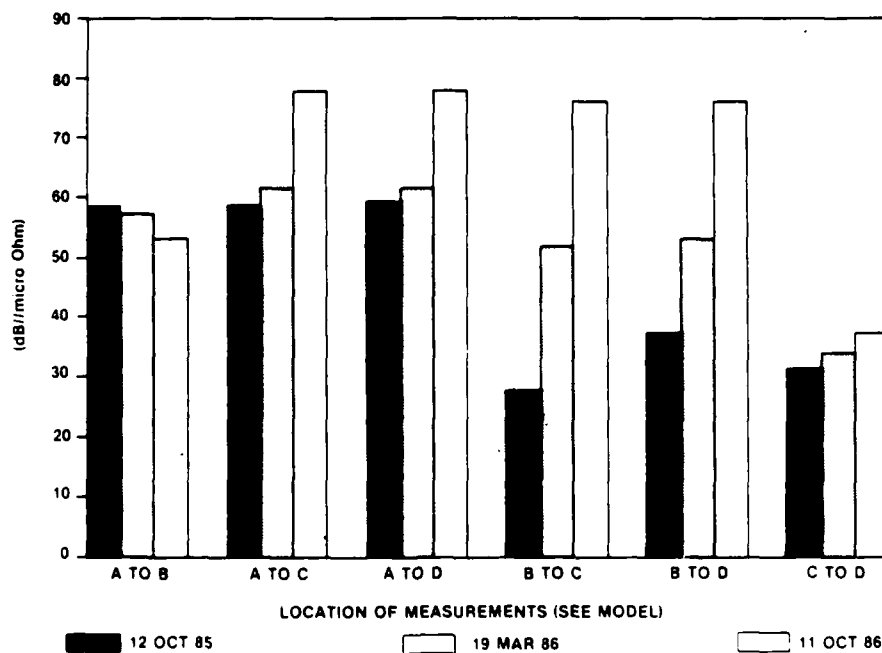


Figure 8: Shipboard D.C. Measurements-vs-Time for the New Smart-Soldered Technology SGA

points illustrated in figure 6. Measurement point A-to-B includes the cable shield and grounding ring(s) or fingered shield contactor to SGA body resistance. Measurement point B-to-C includes the SGA-to-Kickpipe Extension resistance and the resistance associated with the first set of threads. These areas of the SGA are the most significant when considering the SGA's long term performance.

The following observations, taken from the data in figure 7, summarize the long term d.c. performance of the existing (spring) technology SGA:

- a. the d.c. performance of the cable shield and the spring contact portion of the SGA (A-B) actually improved with time (875/225/255 micro-Ohms),
- b. the d.c. performance of the 1st thread interface (B-C) suffered tremendous degradation with time (1.3/9, 300/11, 100 micro-Ohms),
- c. the d.c. performance of the 2nd thread interface (C-D) caused initial degradation (50 micro-Ohms), but it was quickly masked by the high degradation of the first thread interface,
- d. the d.c. performance of the total SGA (A-D) was dominated by the degradation at the thread interfaces, particularly the 1st thread interface. SGA performance degraded from 950 to 9,800 to 11,400 micro-Ohms.

The following observations, taken from the data in figure 8, summarize the long term d.c. performance of new smart-soldered technology SGA:

- a. the d.c. performance of the cable shield and the smart soldered contact portion of the SGA (A-B) improved slightly with time (863/750/463 micro-Ohms),
- b. the d.c. performance of the 1st thread interface (B-C) suffered significant degradation with time (25/400/6600 micro-Ohms),
- c. the d.c. performance of the 2nd thread interface (C-D) was 37.5 micro-Ohms (initially) and a low 7.5 micro-Ohms (finally),
- d. the d.c. performance of the total SGA (A-D) was dominated by the degradation of the thread interfaces, particularly the 1st thread interface. SGA performance degraded from 938 to 1200 to 8100 micro-Ohms.

LONG TERM A.C. PERFORMANCE EVALUATION OF EXISTING & NEW TECHNOLOGY SGAs

As discussed earlier, the a.c. performance of the SGAs could only be evaluated in the laboratory. The kickpipe extensions were fabricated to assist in the removal of the SGAs without affecting their grounding performance.

EXISTING TECHNOLOGY SGA A.C. PERFORMANCE TEST RESULTS

Pre and post installation a.c. performance testing was accomplished using the NUSC test procedure. The results of this testing, conducted 5 hours, 24 hours, and 12 months apart, are shown in figure 9. The range in the short term (hours) test results was discussed at the last IEEE EMC Symposium [2]. Although a function of frequency, the range in

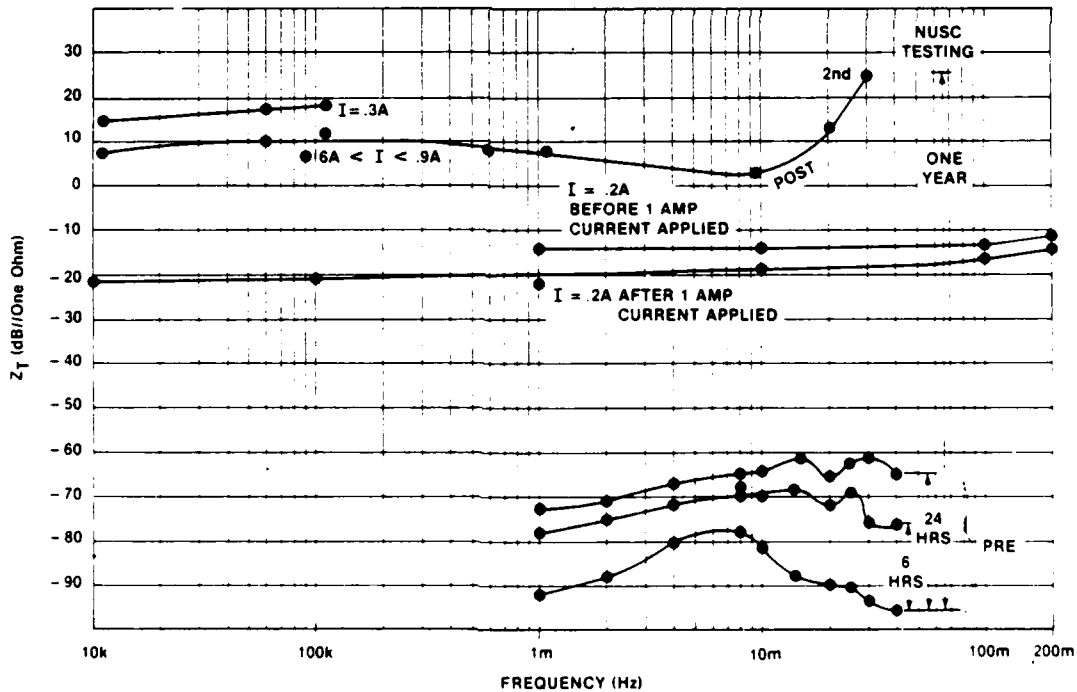


Figure 9: Existing Technology, New Construction SGA A.C. Transfer Impedance: Pre & Post Installation NUSC and 3&2 Test Data

performance nominally ranged from -96 to +24 dB//one-Ohm. This represents a 120 dB range in performance-vs-time. It should also be noted that the performance of the device was dependent on the amount of current driven down the cable shield and the SGA. A 6 to 10 dB increase in the current brought about a 6 to 9 dB increase in the SGA's performance.

G & H also conducted post installation testing on the existing technology SGA. This testing was conducted after the NUSC testing and the test results on the SGA seem to indicate that the SGA may have been physically stressed during shipment and/or testing. The G & H testing shows significantly better test results, ranging from -20 to -30 dB//one-Ohm better than the NUSC testing on the same SGA. We also see that the SGA performance once again varies due to the amount of current driven down the cable shield and SGA. After increasing the current by 14 dB and then retesting with the original current value of .2 amps, the performance improved by approximately 6 dB.

Evaluation of the a.c. performance for the existing technology SGA shows a significant amount of variation between both NUSC pre and post installation test data as well as the G & H post installation test data. This may have been caused by mechanical vibration/stress of the test sample between removal from the ship and between East and West Coast testing. This would tend to suggest that either the kickpipe extension did not work as planned or this SGA's performance is highly dependent on contact resistances/impedances. Hoeft has indicated [7] that "contact impedance is the major electromagnetic hardness degradation factor in cables, connectors, and cableways." It would appear that kickpipe thread areas would have to be added to Mr. Hoeft's list of components having high degradation factors. It was verified earlier in this paper (see figure 4) that a.c. performance testing on the same SGA yielded results within 4 dB of each other when NUSC and G & H test methods were compared. This fact, in addition

to the high degree of correlation to the SGA EMI model developed by Showers [5 & 6], suggests that the measured variation was indeed caused by this type of SGA rather than by the test procedures.

NEW TECHNOLOGY SGA A.C. PERFORMANCE TEST RESULTS

Pre and post installation a.c. performance testing was accomplished using the NUSC test procedure. The results of this testing, conducted 12 months apart, are shown in figure 10. There was no change in performance during the first 24 hrs. The range in the preinstallation a.c. performance was from -85 to -65 dB//one-Ohm. The post installation testing ranged from -55 to -40 dB//one-Ohm. The difference between the curves in figure 10 illustrates a 20 to 30 dB degradation over the one year period of time it was installed on the ship.

G & H also conducted post installation testing on the same new technology SGA. Over a frequency range from 10 kHz to 200 MHz, this testing resulted in SGA performance ranging from -43 to -31 dB//one-Ohm.

Variation in a.c. performance for this SGA indicate significantly less variation between both pre and post installation testing and between NUSC and G & H test data. Therefore, this type of SGA appears to be less susceptible to movement in the cable-SGA-kickpipe assembly.

IMPROVED SOLID CABLE SHIELD CONTACTOR: NEW TECHNOLOGY SGA DEVELOPED

As the existing and the new technology SGAs were environmentally aging on the test platform, an improved new technology SGA was developed. This improved version utilized a new (RG) cable shield contactor that was almost solid as compared to the earlier version that was fingered. Both EMI model and EMI test data indicated that the fingered version caused decreased performance at higher frequencies. Figure 11 illustrates a range of SGA transfer

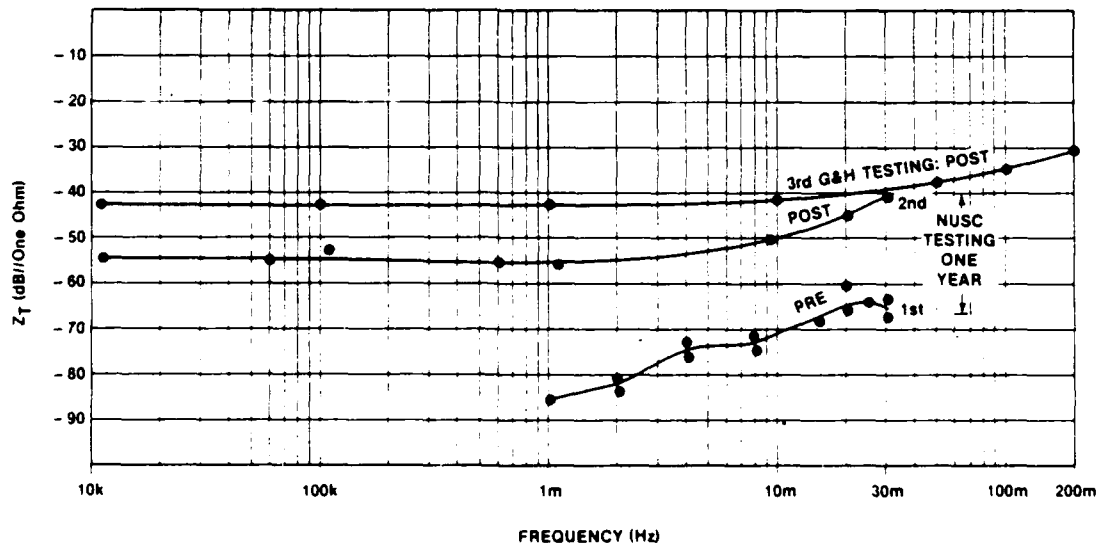


Figure 10: New Technology New-Construction SGA A.C. Transfer Impedance: Pre & Post Installation NUSC and G&H Test Data

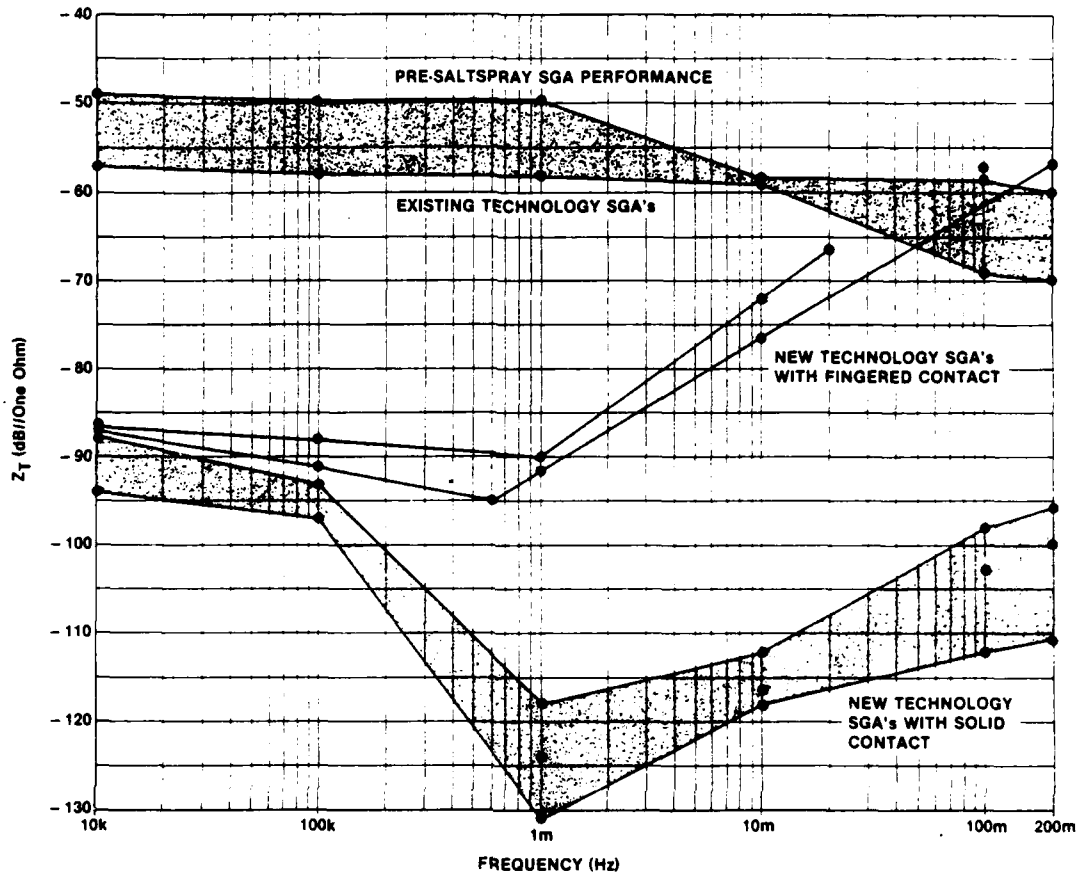


Figure 11: Comparison of Transfer Impedance Test Data For Three Types of RG-214 Style SGA's

impedance (Z_T) test data initially measured on the existing technology SGA (top curves), the new technology SGA (middle curves), and the new technology SGA with the improved cable shield contactor (lower curves). Even with a range of SGA samples tested, it can be seen that the new solid shield contactor dramatically improves the high frequency performance of the SGA.

CONCLUSIONS

- The d.c. performance of the cable shield contact area improved slightly with time for both styles of SGAs.
- the long term d.c. performance of the SGAs was completely dominated by the resistance of the thread interfaces required to connect the SGAs to the ship's hull,
- the spring contact SGA's short-term a.c. performance could be significantly changed by "re-torquing" it,
- the performance of the spring technology SGA showed a variation in performance directly related to the amount of current flowing on the cable's shield (a current increase of 10 dB (NUSC) or 14 dB (G & H) improved performance by

9 or 10 dB, respectively),

- as measured by the NUSC testing, the degradation in performance in the spring contact SGA over time was much worse than the new technology SGA over time (120 dB-vs-44 dB) (+24 to -96 dB) & (-85 dB to -41 dB),
- thread resistance/impedance is a dominant form of degradation not actually within the SGA but one that occurs at the SGA-to-kickpipe interface,
- the d.c. and a.c. performance testing of the new technology SGA occurred on an early device that utilized a "fingered" cable shield-to-SGA contactor; subsequent EMI modelling and testing has indicated that a significant performance improvement (up to 35 dB) can be obtained at higher frequencies when utilizing a "solid" cable shield contactor, and
- it is necessary to consider the life cycle performance of d.c. and a.c. EMI grounds.

RECOMMENDATIONS

- Develop an EMI model to describe the degradation caused by the kickpipe threads; this would have

application for a wide range of EMI grounding devices,

2. Develop an electrochemically compatible solution to the thread degradation problem and evaluate its long term success by shipboard installation and/or accelerated life cycle testing,
3. Develop a military performance specification for the solid cable shield contactor new technology SGA to permit it to be used on a retrofit basis on Naval platforms,
4. Install a new technology SGA, with the solid shield contactor, on a test platform in conjunction with a thread "fix" to ensure that the highest long-term SGA performance is achieved to reduce below-decks electromagnetic (EM) levels caused by EM currents.

ACKNOWLEDGEMENTS

Support for this project was provided by the Office of The Chief of Naval Research/Office of Naval Technology; Submarine Technology Program Element; Program Element Manager is Mr. Gene Remmers, Code 233. Block Program Manager for the Submarine Technology Block Program is Mr. Lincoln Cathers, Code 012.4, of the David Taylor Naval Ship Research & Development Center. Principal Investigator of "The Ships Below-Decks EMC Program" is Mr. David S. Dixon, of the Naval Underwater Systems Center, Code 3431. Triaxial fixture test method and measurement data was provided by Mr. John Miller, consultant.

REFERENCES

1. MIL-STD-1310(E), "Shipboard Bonding, Grounding and Other Techniques for EMC and Safety."
2. David S Dixon & Stanley Sherman, "Reduction of EMI/EMP Shield Currents Using An Improved Shield Ground Adapter," 1986 IEEE International Symposium On EMC, September 1986.
3. H. Kent. "Self Heating/Self Soldering Make-Break Connectors." Electronic Connector Study Group, 18 Nov 1985.
4. M. Van Brunt, "Advanced Current Shunting Device for Shielded Cable and Conduit," 1986 IEEE International Symposium On EMC, September 1986.
5. R.M. Showers and S. Peters, "Development of Models for the Shield Ground Adapter," UPENN RPT MSEE-F-85-3, 31 Dec 1985.
6. R.M. Showers, "Development of a Model for the Shield Ground Adapter," Proceeding of the 1987 IEEE International Symposium on EMC, August 1987.
7. L. O Hoefl, "The Case for Identifying Contact Impedance as the Major Electromagnetic Hardness Degradation Factor," 1986 IEEE International Symposium on EMC, September 1986.

DEVELOPMENT OF A FULL PERFORMANCE COMPOSITE CONNECTOR WITH LONG-TERM EMI SHIELDING PROPERTIES

by

James V. Masi, Member IEEE
Department of Electrical Engineering
Western New England College, Springfield, MA, USA

David S. Dixon, Member IEEE
Naval Underwater Systems Center, New London, CT, USA

Maurice Avoux
formerly of G & H Technology, Inc., Camarillo, CA, USA

ABSTRACT

The purpose of this paper is to discuss two phases of the effort required to develop a full MIL-SPEC connector made from composite materials composed of conducting particles, fibers, or flakes in a matrix of polymeric material. This connector is designed to satisfy a full range of electromagnetic, chemical, and mechanical properties, including corrosion resistance to hostile environments and electrochemical compatibility with electronic cabinets made from aluminum.

The first part of this paper will discuss the factors involved in the composite material/filler selection process, including existing and proposed materials/fillers. The second part will discuss the development of a mathematical model which gives the basis for prediction of some of the electromagnetic properties of a composite material.

Suggestions for further work on materials and modeling are given, with special reference to emerging techniques and materials.

BACKGROUND

Given the crowded electromagnetic environment as well as the potentially hostile land and marine environments existing today, there are many incentives to develop a connector, made from composite polymeric materials, that will have good and non-degrading EMI performance over time. To be useful for a range of applications, the connector must be: resistant to chemical attack, immune to shock (both thermal and mechanical), corrosion resistant when connected to aluminum structures, lightweight, machinable, moldable, capable of operation in high temperature environments (>200°C), and provide better EMI shielding effectiveness (over time) than existing composite technologies. Such were the goals established for the EMI development program.

A cursory evaluation of several ongoing material development efforts indicated that the key to reaching these goals was to assemble a proper mix of technologists who would be capable of developing a full MIL-SPEC connector with performance approaching that of existing metallic connectors. A development team was therefore formed that contained the following expertise:

- a. theoretical electromagnetic interference (EMI) personnel,
- b. theoretical materials personnel,
- c. EMI test personnel, and
- d. connector manufacturing and test personnel.

It was believed that this mix of technologists, all things being equal, would have the highest probability of developing a composite connector with all the desired qualities.

INITIAL RESIN/FILLER SELECTION AND EVALUATION

The high temperature thermoset and thermoplastic resins listed in Table 1 were initially selected for evaluation due to their working temperature, strength, deflection temperature, chemical resistance, and toughness.

RESIN	TEMPERATURE
1. POLYETHERETHERKETONE (PEEK)	232° C
2. POLYPHENYLENE SULFIDE (PPS OR RYTON)	232° C
3. POLYAMIDEIMIDE (PAI)	220° C
4. POLYIMIDE (PI)	204° C
5. POLYETHERSULFONE (PES)	180° C
6. POLYARYLSULFONE (PAS)	180° C
7. POLYETHERIMIDE (PEI)	180° C
8. LIQUID CRYSTAL POLYMER (LCP)	240° C

TABLE 1: POTENTIAL HIGH TEMPERATURE THERMOSETS & THERMOPLASTICS MIL-C-38999, Series IV; MIL-C-28840.

Initially, due to their good electrical conductivity and expected good shielding properties, various combinations and percentages of aluminum flake and fiber were compounded with the above resins. The products were tested and indicated that most of the aluminum/resin combinations suffered from electrical conductivity degradation and significant weaknesses in the injected molded materials. Close investigation indicated that the aluminum filler oxidized very rapidly, especially during temperature cycling, thereby causing a loss in the composite's electrical conductivity, with subsequent loss in both material shielding properties and mechanical properties. Electrical conductivity degraded typically over three orders of magnitude, while mechanical properties had typical degradations of over 30%. This effect is not clearly noted in literature describing the subject[1].

This forced the program into a reevaluation period, in order to discover a metallic or semi-metallic filler or combination of fillers that would not degrade the inherent resin strength and would provide a reasonable amount of electromagnetic shielding that would not degrade with time or temperature. Several promising resin/filler combinations that appear to meet the requirements discussed above have now been compounded. Graphite and nickel coated graphite fibers in these resins were to be used as comparisons for conductivity, corrosion, and modeling, but were not considered to be viable, due to their causal role in the corrosion of aluminum parts in contact with these composites [2].

Resins that were retained for further study include polyimide (PI), polyetheretherketone (PEEK), and polyetherimide (PEI). These resins have good moldability, good to excellent machinability, and have continuous use temperatures exceeding 200°C (loaded). Color was not deemed a determining factor in resin or filler selection.

Fillers presently being evaluated include PAN graphite fibers and flake, nickel coated graphite fibers, carbon particles, indium/tin oxide (ITO) particles, ITO particles with graphite fibers, and aluminum coated E-glass. Early in the study, aluminum coated E-glass proved to be an improper choice due to the chemical tendency of the aluminum to scavenge the oxygen from the underlying glass, causing the aluminum to oxidize and become an insulator rather than a conductor. Mechanical properties were observed to degrade rapidly, causing pullaway of fiber from resin.

The galvanic properties of metals and alloys are given in Table 2 below. The table shows the increasing tendency of the material to corrode as it becomes more anodic.

 < ----- MORE ANODIC

GROUP I	GROUP II
MAGNESIUM	ALUMINUM
MAGNESIUM ALLOY	ALUMINUM ALLOY
ALUMINUM	BERYLLIUM
ALUMINUM ALLOY	ZINC
BERYLLIUM	CHROMIUM
ZINC	CADMIUM
CHROMIUM	CARBON STEEL

MORE CATHODIC ----->

GROUP III	GROUP IV
CADMIUM	BRASS
CARBON STEEL	STAINLESS STEEL
IRON	COPPER & ALLOYS
NICKEL	NICKEL/COPPER
TIN	ITO
TIN/LEAD	MONEL
LEAD	SILVER
BRASS	GRAPHITE
STAINLESS STEEL	RHODIUM
COPPER & ALLOYS	PALLADIUM
NICKEL/COPPER	TITANIUM
MONEL	PLATINUM
ITO	GOLD

TABLE 2: GROUPING OF MATERIALS BY ELECTROCHEMICAL COMPATIBILITY

The unique properties of certain oxides and catalytic-behaving materials to "self-adjust" their electrochemical EMF's (either by oxygen manipulation or other charge transfer) make them extremely attractive in minimizing corrosion due to the dissimilar galvanic potentials. In addition, some of these oxides are semiconductive, allowing for overall improvement of shielding effectiveness (S.E.) when the materials are fabricated into a connector that must be attached to an electronic enclosure. It is also expected that the S.E. of these materials will improve with applied voltage/current, thereby making them perform better during high level electromagnetic field exposure.

Presently, tests are being made on all of the above composite resin/filler variations. Electrochemical tests are being made to verify the expected behavior of these materials when galvanically coupled to aluminum components. EMI shielding, as well as basic complex impedance calculations and tests are being performed to verify models postulated upon distributed parameter calculations. Early results are encouraging and not without the expected undesirable materials interactions between resins and fillers.

The properties of a composite depend on a wide variety of component properties. Among these are relative proportions of resin and filler, size, shape, state of aggregation or agglomeration, relative dispersion, and orientation of filler. Finally, the level of interphase adhesion affects ultimate strength and elongation and is a measure of the unwanted condition of "pullaway". For example, for fibers with circular or square cross-section, one of the simplified methods of predicting the composite modulus, tensile or transverse, (the Halpin-Tsai equation) is:

(1) Tensile: $E_c = V_f E_f + V_m E_m$, and
 (2) Transverse: $E_c = [(1 + 2n V_f)/(1 - n V_f)] E_m$,
 where
 $n = \{[(E_f/E_m) - 1]/[(E_f/E_m) + 2]\}$,

E_c is the modulus of the composite, E_f and E_m are the moduli of the filler and the matrix, respectively, and V_f and V_m are the volume fractions of the filler and matrix, respectively. These are the approximate bases on which the mechanical properties of the ideal composite were pre-estimated.

A THEORETICAL MODEL TO PREDICT THE ELECTROMAGNETIC PROPERTIES OF COMPOSITE MATERIALS

There are a number of theoretical models which conditionally predict the electrical properties of composites based upon a hopping model [3], percolation theory [4], critical loading [5], and simple RC networks [6]. A baseline effort has been made to establish, not only a verifiable model, but one which established the electromagnetic properties of the composite when given a set of specific component material parameters. As a result of the effort, an interactive computer program was written and is evolving, as the model and data dictate, into a tool which will allow for user input of component (fiber and filler) parameters found to be of electromagnetic importance. This program calculates properties from d.c. to one gigahertz, and gives output which can be verified by testing specimens, either in a flanged coaxial holder for shielding effectiveness measurements (Figure 1), in an admittance bridge (Figure 2), or in a network analyzer (Figure 3).

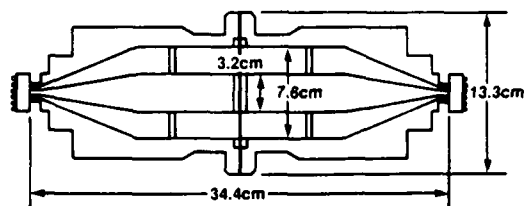


FIGURE 1: FLANGED COAXIAL HOLDER



FIGURE 2: ADMITTANCE BRIDGE



FIGURE 3: NETWORK ANALYZER

The model shows that polymeric composite slabs containing conductive particles, flakes, fibers, or combinations of these, have measurable transmission, reflection, and absorption coefficients. The filler morphology varies characteristics for electromagnetic scattering and absorption in the composite materials. Theoretical results for optimum design of EMI shielding could be derived by using statistical field theory or by distributed parameter network modeling using frequency and field dependent components in the analysis. The model should also be applicable to the construction of radio anechoic chambers and electronic packaging. Two approaches were merged into one to analyze this problem. The stochastic field theory results were superimposed on a conventional three-dimensional impedance model with frequency and field dependent terms [7], [8], [9].

Three factors are prime in the determination of the behavior and properties of composites, both from a mechanical and electrical point of view, exclusive of the approach:

1. The fundamental materials of which the composite is composed;
2. the morphology and structural disposition of the constituents; and
3. The multifactorial interaction among the constituents (e.g. chemical, mechanical, and electrical).

Using the filler model which relates the resistivity of the filler material to that of the composite via the volume fraction of the filler, the d.c. resistivity of the combination can be calculated.

$$(3) \quad \rho + (V_f/3) [1/(1-\sqrt{V_f/3})] \rho_0.$$

Using form factors for the particle, flake, or fiber, and combining this with a three-dimensional matrix, leads to a solvable set of equations involving resistors, capacitors, and inductors at various frequencies and fields. The model needs inputs with respect to electric field and frequency dependence of the resistive and reactive elements, i.e. $R(E, \omega)$ and $X(E, \omega)$. Typical materials are being tested for d.c. and high frequency properties in order to "fit" the functional dependence of $R(E, \omega)$ and $X(E, \omega)$. First iterations are in progress with more sophisticated measurements and model refinements to follow. This extended circuit approach will be later compared with more complex statistical field theory approaches now in progress. It is expected that, at least, a model will be proposed which can serve as a "first test" for new electrical composite formulations.

D.C. CASE

A composite sample under an applied d.c. field has its potential distribution curves bent more drastically over the conducting filler contacts due to space charge. The equivalent circuit representation is shown in Figure 4. Within at least a half order of magnitude, the impedance for a three dimensional array of these components is approximately the value of Z for the simple network. Ignoring, for the time being, distributed parameter considerations, the time constant of such a circuit at a given electric field strength, E , is

$$(4) \quad T = R_0[R(E)C(E)]/[R(E) + R_0],$$

assuming smooth contours on the particle/flake/fiber and an electrically homogenous, isotropic polymer matrix.

A number of researchers have noted that current controlled negative resistance (C.C.N.R.) is observed (voltage dependent threshold initiation) [10]. Local heating of the matrix/conductive filler is deemed to be the cause, the result being quasi-filamentary conduction. This implies that, as the voltage (field) increases across a composite element, its conductivity and, as a result its shielding effectiveness, increases. This effect is enhanced by certain fillers which themselves exhibit C.C.N.R. or voltage controlled negative resistance (V.C.N.R.).

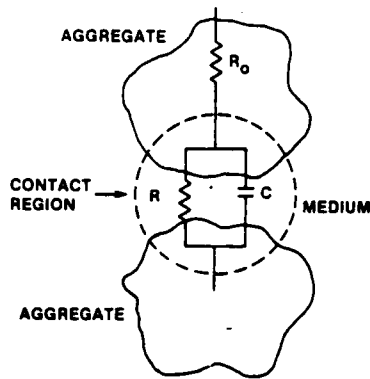
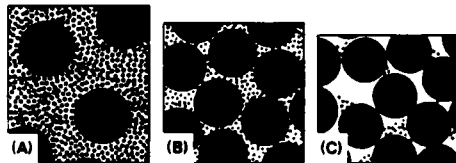


FIGURE 4: EQUIVALENT CIRCUIT

A.C. CASE

Ideally, one would like to see a medium with just the right combination of coarse and fine [11] particles to provide for maximum composite conductivity and maximum mechanical strength, as shown in Figure 5. According to the electrical model shown (ignoring for now the aforementioned inductive component), the equivalent $R_0/R(E,\omega)/C(E,\omega)$ circuit impedance should decrease with increasing frequency. This combined with C.C.N.R. or V.C.N.R. makes the composite with semiconducting particles, flakes, or fibers (or combinations thereof) an improved shield, not only for EMI, but also for electromagnetic pulse (EMP) applications.



(A) excess of fine particles; (B) optimum composition; (C) excess of coarse particles.

FIGURE 5: PACKING OF FINE AND COARSE PARTICLES

Applying the effective medium theory [12] to the conductivity and the complex dielectric constant of the composite material, one can obtain a relationship between the properties of the matrix and those of its components by

$$(5) \quad V_f(\epsilon_f^* - \epsilon_c^*) / (\epsilon_f^* + 2\epsilon_c^*) = - (1 - V_f)(\epsilon_m^* - \epsilon_c^*) / (\epsilon_m^* + 2\epsilon_c^*)$$

where

$$\epsilon_f^*, \epsilon_m^*, \text{ and } \epsilon_c^*$$

are the complex dielectric constants of the filler, matrix, and composite, respectively, and V_f is the volume fraction of the filler.

In general,

$$(6) \quad \epsilon^* = \epsilon' - j\epsilon''$$

where σ is the conductivity in mhos/m, ϵ_0 is the permittivity of free space (approximately 8.85×10^{-12} F/m, ω is the angular frequency in radians/seconds and ϵ is the real, relative dielectric constant. So, the equivalent circuit now becomes a matter of defining a loss tangent of the medium, the dielectric constant of the medium, the conductivity of the flake/fiber/particle, the complex dielectric constant of the filler, the effective morphology of the filler, and the fraction of filler participating in the process. The shape function of the filler is obviously important in the estimation.

RESULTS

Using the form factors for the particle, flake, or fiber involving cross-sectional area considerations of the filler (A), inter-fiber/flake/particle spacing (d), frequency ϵ , resistivity (ρ) as in equation (3), the impedance of the specimen can be expressed by

$$(7) \quad Z = -j / [\rho(\epsilon_0 \epsilon_r A/d) - j(A/\rho d)] + R_0$$

The program written to implement this effort is simple and interactive. The results were compared initially with graphite/PAN fiber samples in polycarbonate and carbon particles in polycarbonate. Measurements of impedance-vs-frequency, for 40 weight percent fiber cylindrical samples are shown in Figure 6. Measurements on the rectangular samples are shown in Figure 7. Table 3 depicts calculated-vs-measured values for impedance and phase angle for cylindrical and rectangular samples of the short fiber variety.

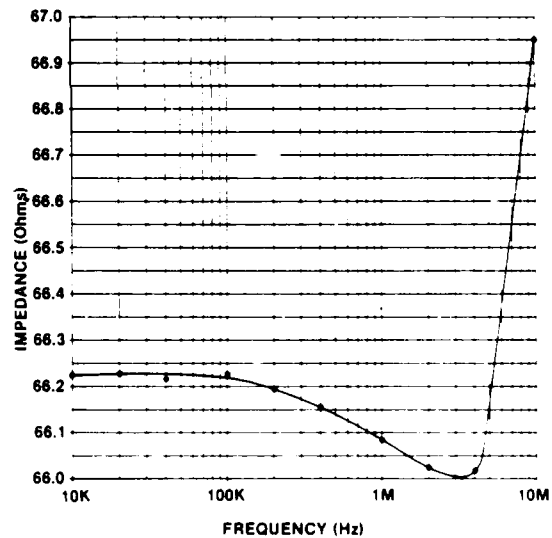


FIGURE 6: MEASURED IMPEDANCE-VS-FREQUENCY FOR CYLINDRICAL SAMPLE OF GRAPHITE IN POLYCARBONATE (0.1V)

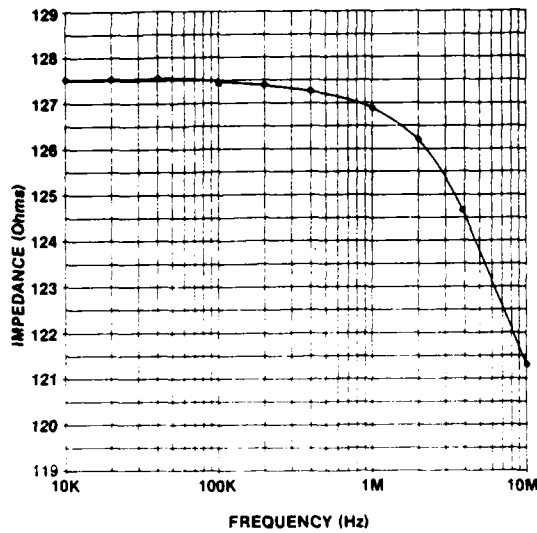


FIGURE 7: MEASURED IMPEDANCE-VS-FREQUENCY FOR RECTANGULAR SAMPLE OF GRAPHITE IN POLYCARBONATE (@.1V)

Frequency	MEASURED	CALCULATED
	$Z(\omega)$ /Phase Angle ($^\circ$)	$Z(\omega)$ /Phase Angle ($^\circ$)
CYLINDRICAL SAMPLE		
10 kHz	66.080/-0.011	155.350/-0.63
100 kHz	66.047/-0.081	158.50 /-1.3
1 MHz	65.933/-0.548	154.330/-4.5
10 MHz	66.951/-3.845	157.550/-7.2
RECTANGULAR SAMPLE		
10 kHz	127.50/-0.014	171.01 /-1.05
100 kHz	127.41/-0.198	192.53 /-3.85
1 MHz	126.90/-1.661	215.80 /-6.88
10 MHz	121.38/-11.574	235.80 /-15.56

TABLE 3. GRAPHITE FIBER COMPOSITE TEST COMPARISON

Samples of 40% graphite fibers and particles were also fabricated in polycarbonate and measured for shielding effectiveness in the ASTM dual chamber box. EMI Shielding for the PAN fibers ranged from 60dB at 15 MHz to 40dB at 1 GHz and from 53dB at 15 MHz to 36dB at 1 GHz. Calculations based upon complex impedance and using the model developed gave values that were 10 to 22% below the measured values for the fiber and 12 to 29% below the measured value for the particles. These values are not vastly different from those found in the literature [13].

CONCLUSIONS

The results shown in Table 3 indicate that there is at least order-of-magnitude agreement with the initial model. However, fiber alignment is extremely important in the calculation and the exact place this alignment factor plays in the model is elusive. Further tests on non-aligned (particle) samples indicate that, at the time of this writing, particulate samples tend to be more predictable than are fiber samples. Though variances are noted in this model, initial results are encouraging in that it appears to

be a parametric model that can predict basic electrical properties of composites, at least at lower frequencies. Other data is being assembled and refinements on the initial model are being made. The authors feel that this approach is indeed a viable one for design and will be pursued by testing and modifications as dictated by results and feedback.

ACKNOWLEDGMENTS

Support for this project was provided by the Office of The Chief of Naval Research/Office of Naval Technology; Submarine Technology Program Element; Program Element Manager is Mr. Gene Remmers, Code 233. Block Program Manager is Mr. Lincoln Cathers, Code 012.4, of the David Taylor Naval Ship Research & Development Center. Principal Investigator of "The Ships Below-Decks EMC Program" is Mr. David S. Dixon, of the Naval Underwater Systems Center, Code 3431.

REFERENCES

1. Nangrani, K.J., "The Effect of Additives and Molecular Weight on Flow and EMI Shielding Properties of Conductive Composites of Polycarbonates", Interference Technology Master, R&B Enterprises, 1986. p.165.
2. Private Communication. M. Avoux, G&H Technology, June, 1986.
3. Mott, N.F., Advanced Physics (Philos. Mag. Suppl.), 16:49 (1967).
4. McCullough, R.L., Composites Science and Technology, 22:3 (1985).
5. Bhattacharya, S.K., "Metal Filled Polymers: Properties and Applications", Marcel Dekker, N.Y., 1986. pp. 170, ff.
6. Sichel, E.K., "Carbon Black-Polymer Composites", Marcel Dekker, N.Y., 1982. pp. 152, ff.
7. Miyazaki, Y., Tominaga, S., and Tanka, M., "Electromagnetic Shield Properties of Plastics and Ceramics with Resistance and Conductance Particles", Tech. Report of IECE. Japan EMC J81-80 (1980).
8. Showalter, R.E. and Snyder, C.H., IEEE Trans. on Circuits and Systems, CAS-33:7, 707-710 (1986).
9. Pike, J.N., Private Communication, UCRI 618 (1970).
10. op. cit. ref. 7, p. 155.
11. Stan, L., Ceramic Bulletin, 65:9, 1293-1296 (1986).
12. Sichel, E.K., et al., J. Electron. Mater. 22:3, 77 (1982).
13. Reilly, J.J., Thoman, S.J., and Lin, W.W., SAMPE Journal, January/February, 1987. pp. 22-27.

CONDUCTED EMISSION MODELS FOR SWITCHING POWER SUPPLIES

by
 Anthony B. Bruno
 Naval Underwater Systems Center
 New London, CT
 203-440-4904

ABSTRACT

Military Standard 461C specifies the limit for harmonic currents generated by electronic equipments in the frequency ranges that cover CE01 emissions (60 Hz - 20 kHz) and CE03 emissions (20 kHz - 50 MHz). These emissions are typical of the electromagnetic interference generated by switching power supplies. A computer model has been developed to study the effect of nonlinear loads on military power distribution systems. Harmonic distortion caused by nonlinear loads is modeled by ideal current sources shunting the appropriate load impedance. The current sources can be given assumed harmonic structures that match measured data. Harmonic voltages and currents are computed at various points in the power distribution system, and the total harmonic distortion is estimated as a figure of merit for the particular configuration. Predicted values of total harmonic distortion will be compared to actual shipboard measurements.

INTRODUCTION

In the past few years much emphasis has been placed on the effects of nonlinear loads on military power distribution systems. Power converters, particularly switching regulators, introduce harmonic currents onto the power distribution system. Harmonic currents introduce many problems including interference with other electronic systems, increased power losses in motors and other magnetic devices, development of secondary harmonic torques that can lead to undesirable machine vibrations, and increased structure currents that flow through input-to-ground capacitors to the ship's ground plane. These harmonic emissions fall into two frequency ranges: 60 Hz - 20 kHz (CE01 emissions) and 20 kHz - 50 MHz (CE03 emissions)^[1]. CE01 emissions are usually related to the rectifier and input smoothing filter, and CE03 emissions are related to the actual switching frequency used in the dc-dc converter. Because many engineers include switching power supplies in their designs, much concern has been expressed about the electromagnetic interference (EMI) caused by these devices on the power distribution systems. Figure 1 shows the harmonic distortion on a laboratory power distribution system. A worst-case computer model has been developed to assess the impact of this EMI on a typical military power distribution system.

Several off-the-shelf power supplies were measured to determine the effects of various types of smoothing filters. Typical switching power supplies use capacitive smoothing filters. These give reasonably good ripple for low cost, weight, and volume. Unfortunately, capacitive smoothing filters become increasingly ineffective at lower frequencies permitting increased harmonic levels to return to the generator and are usually responsible for CE01 emissions failure. Figure 2 shows the spectrum of a three-phase power supply that uses a capacitive type smoothing filter. This spectrum appears flat to some point (the 13th harmonic) and then falls off at $1/n^3$. Several other power supplies were measured and found to have fall-off rates between $1/n$ and $1/n^3$.

Switching power supplies also exhibit conducted emissions in the 20 kHz to 50 MHz range. Designers have typically chosen switching frequencies around 20

kHz because frequencies less than 20 kHz can cause EMI in equipments and are more difficult to filter. Frequencies above 40 kHz can cause additional EMI problems but are easier to filter.

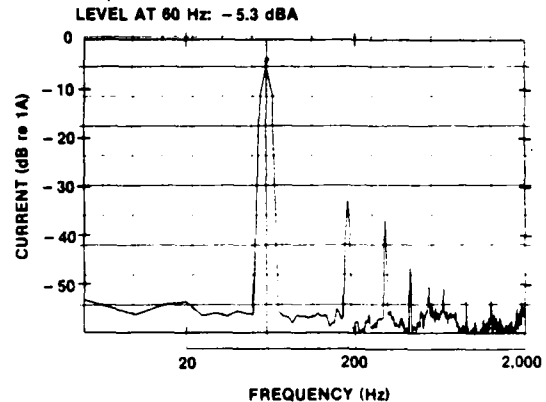


Figure 1. Harmonic Distortion on 60-Hz, Single-Phase Laboratory Powerline

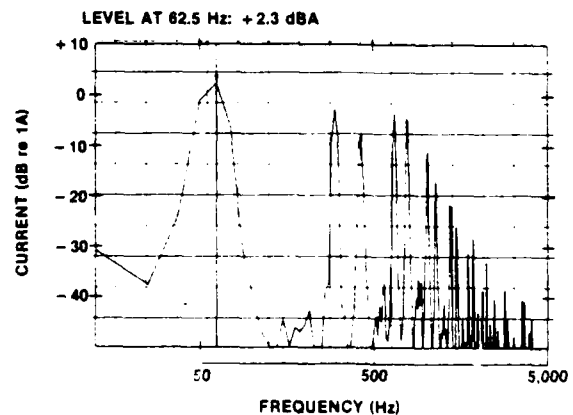


Figure 2. Line Current Spectrum for Phase 1 of the BQQ-5 Type 4B Power Supply

Some manufacturers are producing 100 watt switching power supplies that operate at 200 kHz, but the conducted emissions from supplies in this range are highly dependent upon the filtering provided by the manufacturer. In this study, rather than providing a detailed model for every power supply, a general worst-case switching model has been developed. It is assumed that the filter between the rectifier and the switching circuit has been optimized to provide smoothing, circuit stability, and the necessary rejection at the switching frequency.

Because the primary interest of this study is the effect of the switching regulator on the input power line, only the rectifier, input filter, and the dc to dc converter are investigated. The study included measurements of various rectifier and filter combinations as well as the development of several computer models. In this regard, both forward and backward models were investigated. In both the measurement and forward modeling phases, detailed knowledge of the circuit elements is required. Although this requirement makes forward modeling less useful in EMI analysis, such models nevertheless serve to provide an understanding of the device. In the backward-looking model the nonlinear source is replaced by an equivalent current source with the appropriate harmonic structure. This approach is ideal for EMI analysis because the general characteristics of the switching source are known and can be easily computed. Thus, an EMI model can be constructed that computes the effects of the nonlinear switching power supply without a knowledge of the circuit elements in a specific supply.

COMPUTER MODEL

A new computer program, POWSUP, has been written to predict CE01 and CE03 conducted emissions from switching power supplies. This program is an outgrowth of a program originally written in 1976 to predict total harmonic voltage distortion from nonlinear loads on three-phase power buses^[2]. Similar to its predecessor, POWSUP is an interactive program that asks the user for the various parameters

of the power system to be modeled. Output is returned to the screen where the user can observe the voltages and currents in various locations on the power bus. The total harmonic distortion (THD) is then computed for the range of frequencies specified and for each load in the model. If switching power supplies have been specified as the load, the CE03 currents returned to the generator are also shown. At the end of each model the user is given the option of running another case. Figure 3 is a flow diagram for the computer program.

POWSUP is divided into a CE01 and a CE03 section. The program can calculate harmonic voltages given the configuration of a shipboard powerline. These voltages can be used to predict the THD expected at various locations on the power bus. Harmonic distortion can subject susceptible equipment to voltages that will cause degraded operation. The CS01 specification of MIL-STD-461C^[3] provides the level of voltage required on input power lines to cause degraded operation of susceptible equipment. With this information, the ship designer can identify potential problem areas before the equipment is actually installed on a platform.

THE CE01 MODEL

The computer program models a balanced three-phase wye-wye or delta-delta power distribution system as a single-phase circuit. Harmonic distortion caused by nonlinear loads is modeled by ideal current sources shunting the load impedance. These current sources can be given assumed harmonic structures that match measured data. The model can

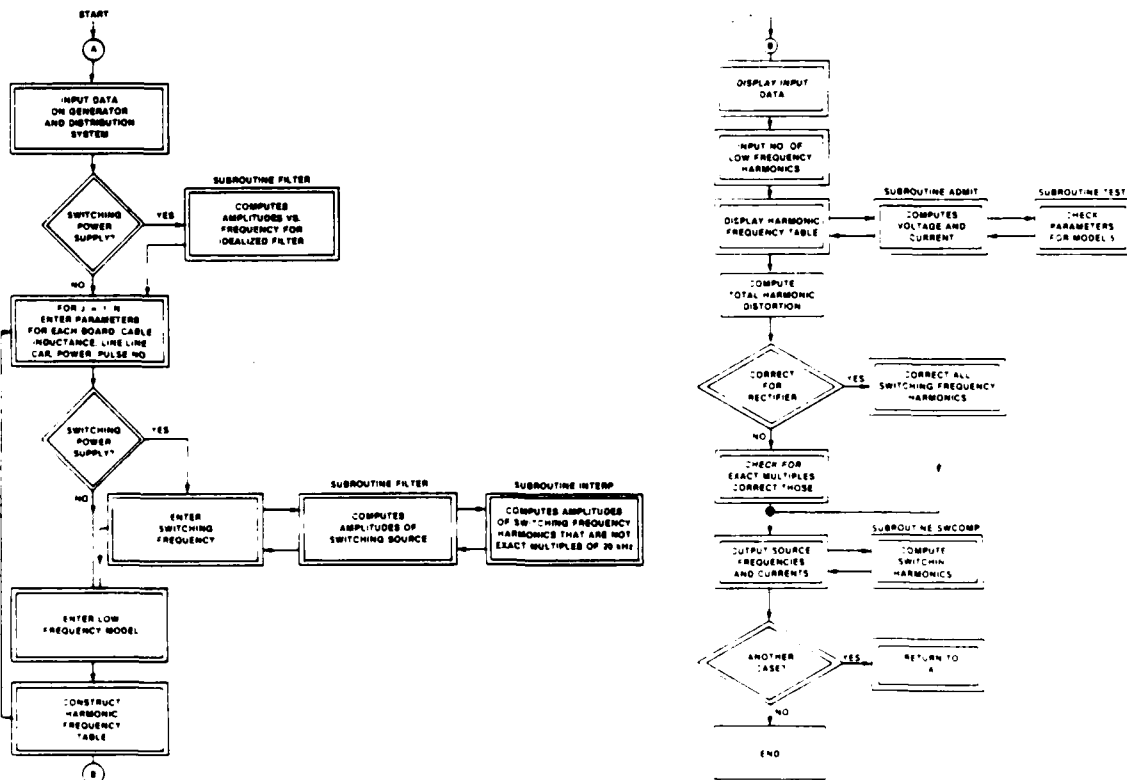


Figure 3. Flow Diagram for Power Supply (POWSUP) Computer Program

analyze up to 10 balanced loads fed in parallel from the generator. Harmonic voltages and currents are computed at various points in the power distribution system, and the total harmonic distortion is estimated as a figure of merit for the particular configuration. The model can accommodate a 60 Hz or 400 Hz generator.

Figure 4(a) shows a typical delta power distribution system and figure 4(b) shows the equivalent wye distribution system. If the systems are balanced then we can write the delta system in its equivalent wye formulation as

$$Z_{an} = \frac{Z_{ab}}{3}$$

$$|I_{an}| = \sqrt{3} |I_{ab}|$$

and

$$|V_{ab}| = \sqrt{3} |V_{an}|$$

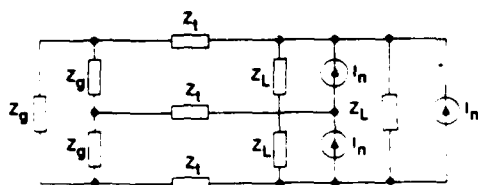


Figure 4(a). Delta:Delta Power Distribution System

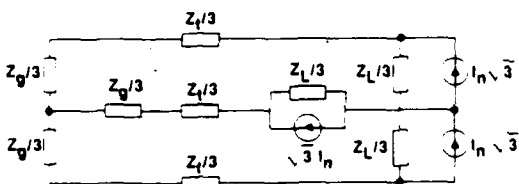


Figure 4(b). Equivalent Wye:Wye Power Distribution System

Each representation has an equivalent formulation for the total power. The total power transferred to the load for the wye distribution is

$$P = 3 |V_{an}| |I_{an}| P_f \tag{1}$$

The power factor, P_f , is assumed to be unity. By substitution of the equivalent V and I in equation 1, the total power transferred to the load in the equivalent delta system can be found. Once the wye formulation has been determined, we need only analyze one leg of the circuit to determine the voltages and currents for the system. Figure 4(c) shows the wye system reduced to one leg.

Figure 5 shows one leg of a power distribution system that has N nonlinear loads in parallel. In order to predict the harmonic distortion due to these loads, the nonlinear loads are replaced by linear current sources whose properties are determined from

$$R = \frac{V_{30}}{P_0} \quad \text{line-to-neutral}$$

and

$$I = \frac{P_0}{V_{30}} \quad \text{line-to-line-current}$$

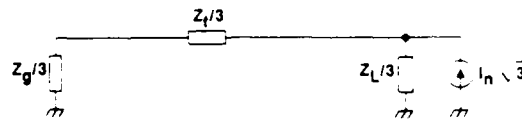
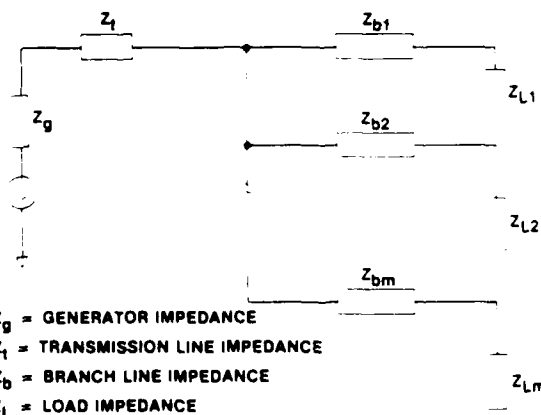


Figure 4(c). One Leg of the Wye Power Distribution System

Figure 4. Power System Configuration, Where Z_g Is Generated Impedance, Z_t Is Transmission Line Impedance, Z_L Is Load Impedance, and I_n Is the Amplitude of the n th Harmonic



Z_g = GENERATOR IMPEDANCE

Z_t = TRANSMISSION LINE IMPEDANCE

Z_b = BRANCH LINE IMPEDANCE

Z_L = LOAD IMPEDANCE

Figure 5. One Leg of a Power Distribution System With m Nonlinear Loads in Parallel

The spectral properties of the current source can be specified as having the following characteristics: $1/n$, $1/n^{1.5}$, $1/n^2$, or 3 percent of the fundamental, or capacitively coupled model. These correspond to fall-off rates of -20 dB/dec, -30 dB/dec, -40 dB/dec, and 0 dB/dec, respectively. The capacitively coupled model represents a flat spectrum to the 13th harmonic and then a fall off of -60 dB/dec. The $1/n$ model represents the inductive filter model where the inductance is very much greater than the critical inductance^[1]. The other models refer to fall-off rates that have been observed experimentally. The 3 percent model is the limit imposed by MIL-STD-461C.

For any source, the amplitude of a given harmonic can be determined from

$$I_n = I_1 SF \frac{1}{n^m}$$

where

n = number of the harmonic,

m = slope of the fall-off rate,

SF = scale factor = 1,

I_1 = amplitude of the fundamental,

and I_n = amplitude of the n th harmonic.

The scale factor parameter allows the flat spectrum model to be implemented. For the 3 percent model, SF=0.03 and $m = 1$. In fact, any flat spectrum model could be implemented with this parameter.

One of the techniques to reduce the amplitude of the low frequency rectifier harmonics is to use multi-phase power supplies. In our model we have assumed that the power system is a balanced three-phase delta connected system. A three-phase full wave rectifier has a pulse rate of 6. This means that the harmonics are related by $n = 1$. Power supplies having higher pulse rates will shift the harmonic frequencies by multiples of six. For example, the first harmonic for a 24-pulse system would be the 23rd. Additional harmonics would be generated according to $24n \pm 1$, for $n = 1, 2, 3, \dots$. Note that $1/23 = 0.04$ is very close to the 3 percent harmonic current limit required by military specification [3]. With the technology already available to implement this technique, it is necessary to analyze nonlinear loads that have pulse rates greater than six.

To compute the harmonic voltages at each load and at the point generator output (see figure 6), the current that returns to the generator from each source must be known. To compute the current, the total admittance of the circuit must be calculated. The following analytical procedure shows how the harmonic voltages and currents are computed.

The variables for each branch at each harmonic frequency are defined as

- V_{g0} = Voltage at the point generator output
- Y_g = Admittance of the generator and transmission line
- A_m = Ratio of the current returning to the generator from the m^{th} branch to the total current of the m^{th} branch or the total admittance of the network as seen from the m^{th} branch
- $I_m'(f)$ = Source strength of m^{th} branch at frequency f
- Y_{rcm} = Admittance of rc network of the m^{th} branch
- Y_r = Sum of the admittance of the branches, excluding the m^{th} branch
- Z_{Lm} = Impedance of the m^{th} load
- Y_m = Admittance of the m^{th} branch
- Z_{bm} = Impedance of the m^{th} branch of the power cable
- C_m = Capacitance of m^{th} branch
- R_m = Resistance of the m^{th} load
- R_{bm} = Resistance of the m^{th} branch of the power cable
- ω_{bm} = Inductance of the m^{th} branch of the power cable
- Z_g = Generator impedance
- Z_t = Transmission line impedance
- R_g = Generator resistance
- L_g = Line-neutral inductance of generator
- R_t = Transmission line resistance
- L_t = Transmission line inductance
- V_t = Voltage of the m^{th} load

The voltage at the point generator output (see figure 6) is

$$V_{g0} = \frac{Z_t f}{Z_g + Z_t} I_g$$

where

$$I_g = \sum_{m=1}^M A_m f I_m'(f)$$

is the total current that returns to the generator of frequency f and

$$A_m = \frac{Y_m}{Y_{rcm} + Y_r + Y_m}$$

is the total admittance of the network as seen from the m^{th} branch. The various individual admittances are given by,

$$Y_r = \sum_{m=1}^M A_m Y_m(f), \quad A_m = \begin{cases} 1 & m \neq r \\ 0 & m = r \end{cases}$$

$$Y_m(f) = \frac{Y_{rcm}(f)}{Z_{bm}(f)Y_{rcm}(f) + 1}$$

$$Y_{rcm} = \frac{j\omega C_m R_m + 1}{R_m}$$

The impedance of the m^{th} branch Z_{bm} (see figure 6) is given by,

$$Z_{bm} = R_{bm} + j\omega L_{bm}$$

The admittance of the generator is

$$Y_g = \frac{1}{Z_g + Z_t}$$

where

$$Z_g = R_g + j\omega L_g$$

and

$$Z_t = R_t + j\omega L_t$$

Finally, the voltage at the m^{th} load can be found from

$$V_m = Z_{bm} I_m' \sqrt{2} + V_{g0}$$

This is an approximation of the true voltage, as shown in figure 6. The nonlinear load could easily have been represented with the current source in series with the load; in this case, the equation for the voltage would be exact. Therefore, as a first approximation, it is assumed that the voltage distortion at the load depends only on the voltage drop on the branch connected to that load, plus the voltage distortion due to the harmonic currents returning to the generator. Note that in this particular model, R_{bm} , R_t , and R_g are assumed to have zero line resistance, which is a good approximation for low frequency harmonics.

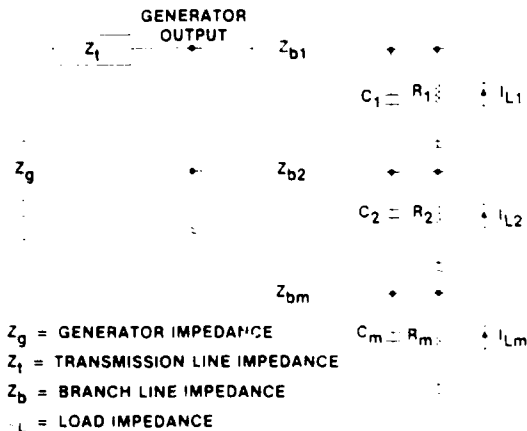


Figure 6. The set of a Power Distribution System with nonlinear loads, analyzed by a linear current source.

The THD is computed using an approximation of its standard definition by the Institute of Electrical and Electronics Engineers (IEEE) [3]. Thus, for a three-phase nonlinear source, the THD is

$$THD = \frac{\sqrt{\frac{V_4^2}{5} + \frac{V_5^2}{7} + \frac{V_{11}^2}{11} + \frac{V_{13}^2}{13}}}{V_1} \cdot 100 + 1\%$$

where V_1 is the rms voltage at the fundamental. The 1 percent is added to account for the harmonic voltage distortion attributable to the generator.

In summary the CEO1 model includes multi-phase power supplies, up to 100 harmonics of the fundamental for a six-pulse rectifier (the number of harmonics for higher pulse numbers is determined from $\frac{600}{P}$ where P is the number of pulses), choice of five harmonic fall-off models, including a model for capacitively coupled power supplies, computation of CEO1 conducted emissions current that return to the generator at each harmonic, computation of THD for all harmonics, error trap routines, and the ability to cycle through the program to run multiple cases.

CEO3 EMISSION MODEL

The model for switching power supplies replaces the nonlinear load with a linear current source having spectral characteristics similar to the load it is replacing. The CEO3 current source would be in parallel with the CEO1 source and would have infinite impedance. This is necessary to prevent current from the CEO1 source from seeing an additional branch. The new current source would replace the smoothing filter as well as the switching circuits. This is all that is necessary to model because most switching regulators are transformer coupled for dc-dc isolation. The impedance of this second source would effectively be the resistive component computed from the output power, or

$$R = \frac{V_{30}^2}{P_0}$$

The characteristics of the smoothing filter are taken into account in the computation of the amplitudes of the harmonics for this source.

The characteristics of the CEO3 current source can be found by assuming a worst-case model first introduced by Kamm [6,7] in 1978. Figure 7 shows a simplified model of the worst-case switching topology, which is the buck converter. Here the two-pole switch represents the switching transistor that turns the input current on and off, resulting in a square wave on the input side of the device. The diode maintains current in the load while the switch is off. However, the switching transistor has a finite rise and fall time; typical switching transistor rise times are on the order of 100 ns.

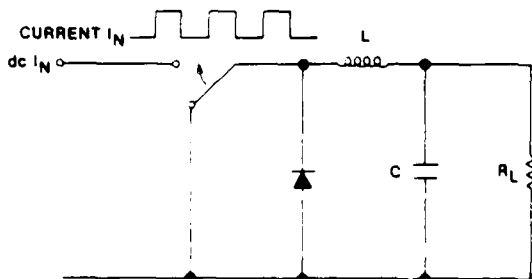


Figure 3. Simple Model of Switching Power Supply, Single Buck Topology

Thus, in this model, the switching source is replaced by a symmetrical trapezoidal periodic waveform. Figure 3(a) shows the waveform for the proposed current source. The normalized Fourier coefficients for an infinite train of symmetrical trapezoidal pulses are

$$C_n = \frac{2}{(n\pi)^2} f_{tr} \sin[n\pi f(t_0 + t_r)] \sin(n\pi f t_r)$$

where the constants are defined in figure 3(a).

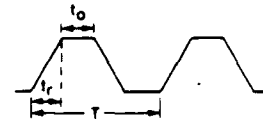


Figure 3(a). Trapezoidal Wave with period $T = 60 \mu\text{sec}$, rise time $t_r = 30 \text{ nsec}$, and duty cycle $t_0 = 25 \mu\text{sec}$

In order to more accurately model the waveshape of the switching current, the turn-on spike of the diode recovery current can also be included. The diode recovery spike is modeled as a pulsed, critically damped, exponentially decaying sine wave. Because the total waveform is the summation of two independent effects, the waveforms can be analyzed separately in the frequency domain. Figure 3(b) shows the waveform of the pulsed exponentially decaying sine wave and is represented by,

$$f(t) = e^{-at} \sin bt$$

where

a = damping factor

$b = 2\pi f_0$, and

f_0 = frequency of the sine wave.

The Fourier coefficients for the waveform shown in figure 3(b) can be found by integrating $f(t)$ over the period by

$$C_n = \frac{1}{T} \int_0^T f(t) e^{-j2\pi n t} dt$$

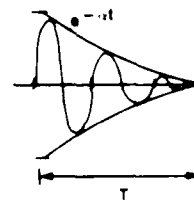


Figure 3(b). Pulsed Exponentially Decaying Sine Wave where $T = 60 \mu\text{sec}$, $f_0 = 3 \text{ MHz}$, $a = 1.1 \times 10^7 \text{ sec}^{-1}$, and $t = 60 \mu\text{sec}$

The integration gives the normalized coefficients as

$$c_n = \frac{1}{2jT} \left(\frac{e^{Z_2 t} - 1}{Z_2} - \frac{e^{-Z_1 t} - 1}{Z_1} \right)$$

where

$$Z_1 = \alpha - j(\beta - 2n\pi f_0)$$

and

$$Z_2 = \alpha + j(\beta + 2n\pi f_0)$$

The combined waveform for the trapezoidal switching current with diode recovery spike is shown in figure 9. The resultant Fourier transform is also shown in this figure. This plot is for a switching frequency of 20 kHz, rise time of 30 ns, and a 1 amp turn-on spike. This curve serves as the basis for our model. Kamm [6] gives the characteristics of an idealized smoothing filter, and this filter has been implemented into the model to compute the estimated amplitudes of the CE03 current source. Figure 10 shows the characteristics of this filter, and figure 11 shows the estimated amplitude of a 1 amp switching source at 20 kHz reflected through the smoothing filter. These estimates agree very well with those shown in reference 6 for similar waveforms. Note that in this new model, switching frequencies up to ≈ 100 kHz are allowed. For switching currents greater than 1 amp, the amplitudes can be scaled by,

$$R_x = 20 \text{ Log}(I_x)$$

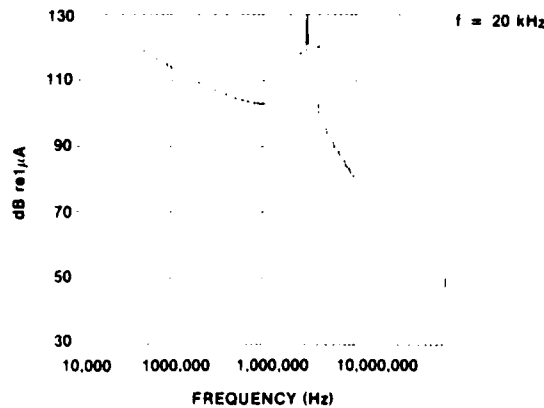


Figure 9. Fourier Coefficients for 20-kHz Trapezoidal Wave with Diode Recovery Spike

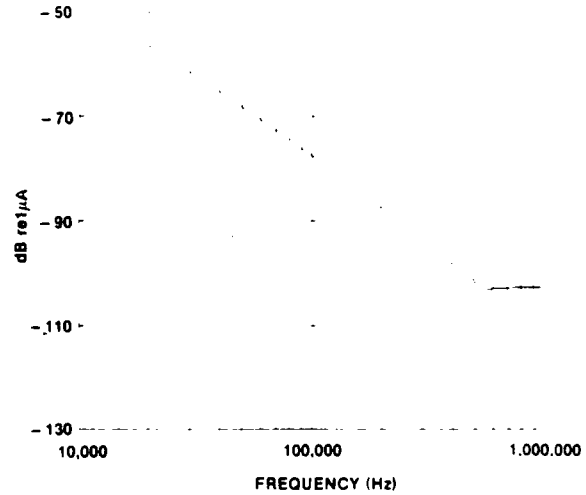


Figure 10. Idealized Smoothing Filter

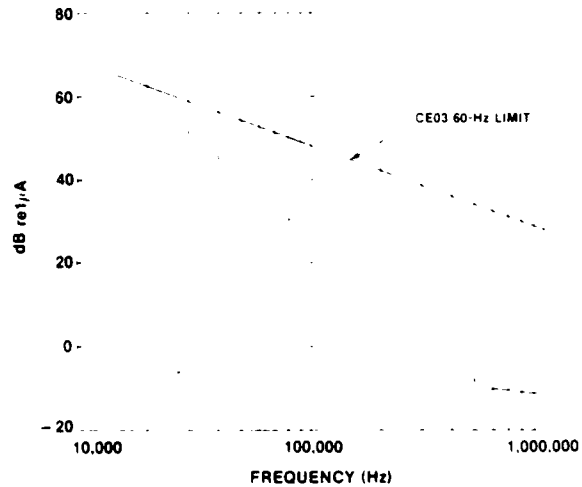


Figure 11. Estimated Amplitude of Switching Source Model at 20-kHz Reflected Through Smoothing Filter. Also shown is the CE03 limit line for a 60-Hz load current $\leq 1A$ narrow band. Note that the CE03 limit line is not shown above 1 MHz.

SAMPLE POWER SUPPLY RUNS

In this section, sample runs are used to illustrate the capability of the computer model using a hypothetical power distribution system. Total harmonic distortion and return currents are computed for various pulse rate systems. The computer model is also compared to shipboard measurements taken on a 43.2-kw motor generator, 400-Hz power distribution system. Measured and computed THD are shown for various loads on the power distribution system.

Hypothetical Power Supply Runs

Because the low frequency conducted emissions dominate harmonic distortion on the power bus, the effect of using multiphase power supplies will be the first example shown. Figure 12 shows a 135-kw, 400-Hz power distribution system with six nonlinear loads. Table 1 compares the THD at the point generator output for various multiphase supplies; all the sources are assumed to have a 1/n fall off, 0° firing angle, and instantaneous commutation.

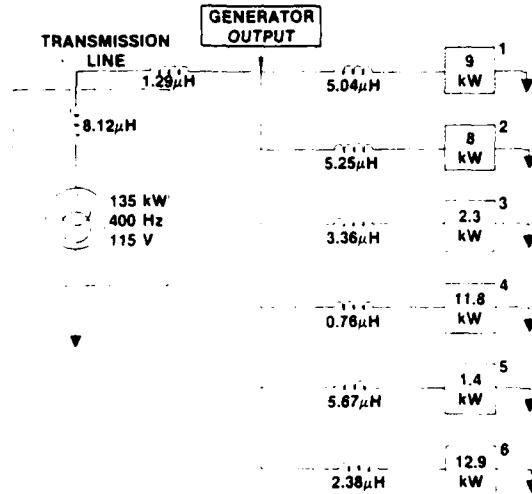


Figure 12. Hypothetical Powerline Configuration

Clearly, as the pulse number increases, the THD decreases. In fact, for 18-pulse supplies, the THD is almost 5 percent, which is the limit for voltage distortion, and for 24-pulse supplies, the THD is below the limit. However, the real problem with harmonic current is not the type of distortion, but the magnitude of current flowing at the various frequencies back to the generator. Table 2 shows the current that returns to the generator for the various pulse numbers. Note the particularly high currents that are flowing in the VLF range. If these currents are allowed to flow on the structure through line-to-ground filters, large magnetic fields, which could interfere with sensitive equipment or low level signal transmission lines, would be generated. Structure currents are known to be a significant problem, particularly in the VLF range.

Table 1. Comparison of Total Harmonic Distortion (THD) at Point Generator Output for Multiphase Supplies

Pulse No.	THD (%)
6	9.5
12	6.4
18	5.1
24	4.3

Table 2. Predicted CEOI Currents Returning to Generator for Various Pulse Numbers

Frequency (Hz)	Current (A)			
	6 PULSE	12 PULSE	18 PULSE	24 PULSE
2000	41.8			
2800	27.8			
4400	15.0	15.0		
5200	11.6	11.6		
6800	7.5		7.5	
7600	6.2		6.2	
9200	4.4	4.4		4.4
10000	3.8	3.8		3.8
14000	2.4		2.4	
14800	1.8		1.8	
18800	1.2	1.2		1.2
19600	1.1	1.1		1.1

Shipboard Run

As a final study, shipboard data will be compared with predicted data; figure 13 shows the power distribution system for the shipboard data. In this experiment, the THD was measured for various loads on the 400-Hz, 43.2-kw power distribution system. An attempt was made to model the various sources with the appropriate fall off; however, often the measured harmonic fall off was between the models available. In those cases, the model that provided the best fit was chosen. Line-to-ground capacitance was included when the data were available. Table 3 summarizes the measured data, comparing the predicted THD with measured values. All loads were six-pulse sources. The data shown in the table, although by no means exact, are close enough to indicate that the chosen model is a good first attempt at predicting the expected THD. Table 4 shows the expected currents that return to the generator from these loads. These data were computed under the same conditions as those in table 3. The currents shown in table 4 are by no means insignificant; if allowed to flow through the structure, they would cause considerable interference. One way to control the propagation of such structure currents is to provide isolation for all nonlinear equipments. Although this works well in controlling structure currents, the extra weight and expense to provide this isolation are prohibitive.

Table 3. Comparison of Measured and Predicted Values of Total Harmonic Distortion (THD) from the Shipboard Data

Load	Measured THD (%)	Predicted THD (%)	Model No.
1	3.3	5.00	1
2	3.4	5.01	1
3	4.2	5.02	1
4	3.54	5.03	1
5	3.76	4.99	1
6	4.39	5.15	1
7	3.94	5.14	1

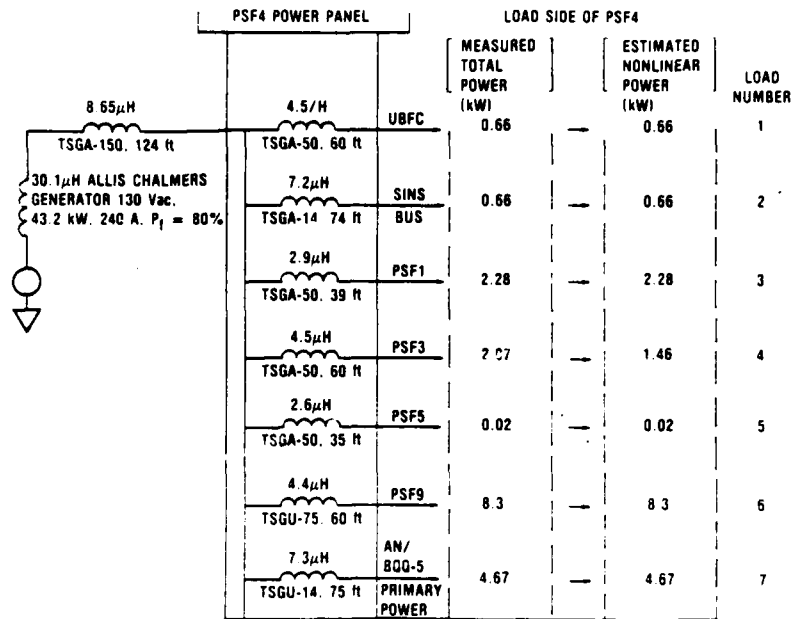


Figure 13. Model of the 43.2-kW, 400-Hz shipboard power Distribution System

Table 4. Predicted Emission Currents Returning to Generator From the Shipboard Data

Frequency (Hz)	Current (A)
2000	7.0
2800	3.9
4400	1.6
5200	1.1

CONCLUSIONS

Harmonic distortion models for switching power supplies were investigated for 60 Hz to 50 MHz frequency range. A computer program has been developed to incorporate both low CEO1 and high CEO3 frequency sources. It computes conducted emission currents that return to the generator in both frequency ranges for various nonlinear loads. These loads can be arranged in any way desired, can have various pulse rates, and can utilize dissipative or switching power supplies. The results have been shown to agree well with actual measurements from shipboard power distribution systems. The program can be used as an effective design tool for predicting the worst-case level of harmonic distortion from nonlinear loads on proposed power distribution systems. Such data are invaluable to the design engineer who needs familiarity with the effects of nonlinear high power loads on a power distribution system, but does not need an extensive knowledge of each load.

ACKNOWLEDGEMENTS

Support for this project was provided by the Office of The Chief of Naval Research/Office of Naval Technology; Submarine Technology Program Element; Program Element Manager is Mr. Lincoln Cathers, Code 233. Block Program Manager for the Submarine Technology Block Program is Mr. Gene Remmers, Code 012.4, of the David Taylor Naval Ship Research and Development Center. Principal Investigator of "The Ships Below-Decks EMC Program" is Mr. David S. Dixon, Naval Underwater Systems Center, Code 3431.

REFERENCES

1. Military Handbook, Design Guide for Electromagnetic Interference (EMI) Reduction in Power Supplies, MIL-HDBK-2419, Sept 1983.
2. D.S. Dixon, "Modeling and Predicting Power System EMI and Input Line Distortion," Proceedings of the Tenth International Solid-State Power Electronics Conference, Powercon 10, 21-25 March 1983.
3. Military Standard, Electromagnetic Emission and Susceptibility Requirements for the Control of Electromagnetic Interference, MIL-STD-461C, 4 Aug 1986.
4. R.J. Distler and S.G. Monshi, "Critical Inductance and Controlled Rectifiers," IEEE Trans on Industrial Electronics and Control Instrumentation, vol. IECE-12, p34-37, March 1965.

5. IEEE Guide for Harmonic Control and Reactive Compensation of Static Power Converters, IEEE STD 519-1981, The Institute of Electrical and Electronics Engineers, Inc., New York, NY, 27 April 1981.
6. F. Kamm, "Design Techniques to Limit EMI from Switching-Mode Converters," Proceedings of the Sixth National Solid-State Power Conversion Conference, Powercon 6, May 1979.
7. E. Kamm, "New Military EMI Specifications Affecting the Input Circuit Architecture of ac to dc Converters," Proceedings of Powercon 8, The Eighth National Solid-State Power Conversion Conference, 28 April 1981.

CROSSTALK IN COAXIAL TRANSMISSION SYSTEMS

Steven J. Peters and Ralph M. Showers
 Moore School of Electrical Engineering
 University of Pennsylvania
 Philadelphia, PA 19104-6390

Abstract

The crosstalk between two parallel braided shield coaxial cables is examined. A comparison is made between the existing transmission line model, traditionally used for analyzing such coupling, and a new integral equation formulation. Measurements of the far-end crosstalk (FEXT) were made and the correlation of this data with these two theories is discussed. In particular, it was found that, at high frequencies, the integral equation approach was much more accurate at predicting the crosstalk than transmission line theory.

1. Introduction

Models currently available in the literature for describing crosstalk between two parallel coaxial cables are based on the premise that the coupling occurs via a two wire transmission line which consists of the cable shields [1-5]. For the case where the shield ends are shorted together, measurements of the far-end voltage transfer ratio up to a frequency of 1 GHz have been reported and this data agrees with the theoretical calculations [2]. The measurements, however, were performed only for small cable separations and no attempt was made to determine the crosstalk as a function of cable separation.

In this paper the crosstalk between two coaxial cables is calculated based on a new concept. Namely, the shield of a coaxial cable can be modeled as a transmitting linear antenna with driving sources on this antenna arising from electric and magnetic field leakage through the shield. The crosstalk between two coaxial cables is then calculated using an integral equation approach.

2. Formulation of the Problem

In developing a theoretical model for the crosstalk between coaxial cables, the idealized configuration of Fig. 1 is considered. This configuration was chosen because it exhibits a number of the basic principles involved with such coupling. Here the source cable is infinite in length and its outer conductor is a flexible braid. The receptor cable is

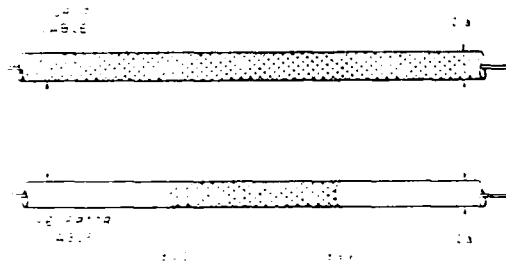


Fig. 1. Idealized Infinite Cable Configuration.

also infinite in length, but is braided only over a finite section of length L. The rest of the receptor cable shield is solid metal. In general the radii of the cables need not be equal, but are assumed as such for analytical convenience. Also, the shield radii are assumed to be small with respect to a wavelength such that $k_0 a \ll 1$ where a is the shield outer radius and k_0 is the free space propagation constant. In addition, any currents induced along the outside of the cable shields are assumed to be circularly symmetric. These assumptions comprise the thin wire approximation and as a consequence of this we need only consider electric field components parallel to the cable axis.

Throughout this paper a time dependence of $\exp(j\omega t)$ is assumed, but suppressed.

3. Transmission Line Solution for the External Shield Currents

In transmission line crosstalk theory the shields of the two cables are treated as a two wire line and this two wire line is driven by field leakage from the source cable. This leakage is modeled by a distributed voltage and current source along the two wire line [3]. In the present case both cables are infinite in length and these sources are given by

$$E(z) = Z_t I_s \exp(-j\beta z) \tag{1}$$

and

$$J(z) = -Y_t V_s \exp(-j\beta z) \tag{2}$$

respectively, where Z_t is the surface transfer impedance, Y_t is the transfer admittance, I_s is the current amplitude along the inside surface of the source cable shield, V_s is the amplitude of the voltage difference between the shield and the center conductor of the source cable, β is the propagation constant inside the cable, and losses along the inside of the source cable are assumed to be negligible.

The expression for the current distribution along a transmission line excited by distributed sources is well known and is given by [6]

$$I(z) = [Q_V(z) + P_V(z) Z_{0S}] \exp(-\gamma z) + [Q_V(z) + P_V(z) Z_{0S}] \exp(\gamma z) \tag{3}$$

where Z_{0S} is the characteristic impedance of the two wire line consisting of the cable shields, $\gamma = \alpha + j\beta$ is the propagation constant of the two wire line, and

$$P_V(z) = \frac{1}{Z_{0S}} \int_{-L}^L \exp(-\gamma s) E_2(s) ds \tag{4}$$

$$Q_V(z) = \frac{1}{Z_{0S}} \int_{-L}^L \exp(-\gamma s) E_2(s) ds \tag{5}$$

$$P_c(z) = \frac{Z_0 s}{2} \int_{-\infty}^{\infty} \exp(\gamma s) J(s) ds \quad (6)$$

$$Q_c(z) = \frac{Z_0 s}{2} \int_{-\infty}^{\infty} \exp(-\gamma s) J(s) ds \quad (7)$$

In using this solution, initially the cables are assumed of length L. After a solution is obtained the limit is taken such that L goes to infinity.

Using eq.'s (1), (2), and (4) through (7) in eq. (3), the transmission line solution for the external shield current is obtained as

$$I_t(z) = \frac{-I_0}{2} \frac{s}{-B} \frac{Z_0 j k_0}{Z_0 s} [Y_t Z_{os} j \beta] \exp(-j \beta z) \quad (8)$$

In obtaining eq. (8), since the losses are small, any terms proportional to α are neglected.

4. Integral Equation Solution for the Induced External Shield Currents

In the integral equation approach the source cable is modeled as a thin linear antenna with driving sources on this antenna resulting from the coupling mechanisms of Z_t and Y_t . These sources excite currents along the outside of the source cable shield producing an external field which is impressed on the receptor cable shield. This impressed field in turn induces a current along the outside of the receptor cable shield and, through the mechanisms of Z_t and Y_t , voltages are induced on the inside of the receptor cable.

Note that the current induced on the receptor cable shield causes a field to be impressed back on the source cable shield and this interaction between the two cables must be taken into account. This is accomplished by simultaneously solving a pair of coupled integral equations for the currents on both cables.

To derive the required integral equations we start with the magnetic vector potential. The relationship between the magnetic vector potential, which arises due to the current on a small diameter cable shield or thin wire, and the corresponding longitudinal electric field is given by [7]

$$E_z = \frac{-1}{j \omega \mu_0 \epsilon_0} \left[\frac{1}{r} \frac{\partial}{\partial r} \left(r \frac{\partial}{\partial r} \right) + \frac{\partial^2}{\partial z^2} \right] A_z \quad (9)$$

and at the surface of a thin wire we have [7]

$$E_z = \frac{1}{j \omega \mu_0 \epsilon_0} \left[\frac{\partial^2}{\partial z^2} + k_0^2 \right] A_z \quad (10)$$

Since the braided shields are considered to be good conductors any fields at the surface due to a surface impedance can be neglected. The boundary condition at the surface of the source cable shield is then

$$E_{z1} + E_{zr1} + E_{zr2} = 0 \quad (11)$$

where E_{z1} is the impressed field due to leakage through the source cable shield, E_{zr1} is the corresponding induced field from the external shield currents, and E_{zr2} is the impressed field which arises due to the currents induced on the receptor cable shield. Substituting

eq. s. (9) and (10) for the corresponding quantities in eq. (11) we obtain

$$-j \omega \epsilon_0 E_{z1} = \left[\frac{\partial^2}{\partial z^2} + k_0^2 \right] A_{z1} + \frac{1}{r} \frac{\partial}{\partial r} \left(r \frac{\partial}{\partial r} \right) A_{z2} \quad (12)$$

where A_{z1} is the magnetic vector potential due to the external current on the source cable shield, and A_{z2} is the magnetic vector potential due to the external current on the receptor cable shield. A similar equation for the receptor cable shield is also obtained. In this case, however, weak coupling is assumed and the field leakage from the inside to the outside of the receptor cable is neglected. Therefore, we have

$$0 = \left[\frac{\partial^2}{\partial z^2} + k_0^2 \right] A_{z2} + \frac{1}{r} \frac{\partial}{\partial r} \left(r \frac{\partial}{\partial r} \right) A_{z1} \quad (13)$$

Under the thin wire approximation the magnetic vector potentials are given by [7]

$$A_{z2} = -j \int_{-\infty}^{\infty} I_2(s) G_2(z,s) ds \quad (14)$$

$$A_{z1} = -j \int_{-\infty}^{\infty} I_1(s) G_1(z,s) ds \quad (15)$$

where

$$G_2(z,s) = \frac{\exp(-jk_0[(s-z)^2 + a_2^2]^{1/2})}{4\pi[(s-z)^2 + a_2^2]^{3/2}} \quad (16)$$

$$G_1(z,s) = \frac{\exp(-jk_0[(s-z)^2 + a_1^2]^{1/2})}{4\pi[(s-z)^2 + a_1^2]^{3/2}} \quad (17)$$

Substituting eq.'s (14) and (15) into eq.'s (12) and (13) and rearranging, the coupled integral equations for the external shield currents are obtained as

$$j \omega \epsilon_0 E_{z1}(z) = - \left[\frac{\partial^2}{\partial z^2} + k_0^2 \right] \int_{-\infty}^{\infty} I_1(s) G_1(z,s) ds \quad (18)$$

$$+ \frac{1}{r} \frac{\partial}{\partial r} \left(r \frac{\partial}{\partial r} \right) \int_{-\infty}^{\infty} I_2(s) G_2(z,s) ds$$

$$0 = - \left[\frac{\partial^2}{\partial z^2} + k_0^2 \right] \int_{-\infty}^{\infty} I_2(s) G_2(z,s) ds \quad (19)$$

$$+ \frac{1}{r} \frac{\partial}{\partial r} \left(r \frac{\partial}{\partial r} \right) \int_{-\infty}^{\infty} I_1(s) G_1(z,s) ds$$

The object now is to solve eq. s. (18) and (19) for the external shield currents I_1 and I_2 . This

is accomplished by using Fourier transforms. Since the integrals are convolution integrals their Fourier transforms are easily obtained. Therefore, Fourier transforming eq. (18), and cancelling like factors on both sides of the equation, we obtain

$$\tilde{I}_1(k)H_0[a\xi] + \tilde{I}_2(k)H_0[r\xi] = \frac{4\epsilon_0}{\xi} \tilde{E}_{z1}(k) \quad (20)$$

where $\xi^2 = (k_0^2 - k^2)$ is positive when $k_0^2 > k^2$ and negative imaginary when $k_0^2 < k^2$. The transform variables are k and z and a tilde over a quantity denotes its Fourier transform. A similar analysis of eq. (19) results in

$$\tilde{I}_1(k)H_0[r\xi] + \tilde{I}_2(k)H_0[a\xi] = 0 \quad (21)$$

In obtaining eq.'s (20) and (21) the formulas

$$\frac{\partial}{\partial r} H_0[r\xi] = -\xi H_1[r\xi] \quad (22)$$

$$\frac{\partial}{\partial r} H_1[r\xi] = \xi H_0[r\xi] - \frac{1}{r} H_1[r\xi] \quad (23)$$

have been used. Here H_0 and H_1 are zero and first order Hankel functions of the second kind.

Expressions for $I_1(z)$ and $I_2(z)$ are obtained by solving eq.'s (20) and (21) for $\tilde{I}_1(k)$ and $\tilde{I}_2(k)$ and inverse Fourier transforming. The actual expressions depend on the form of $\tilde{E}_{z1}(z)$, but in general are given by

$$I_1(z) = -4\epsilon_0 \frac{1}{2\pi} \int_{-\infty}^{\infty} \frac{\tilde{E}_{z1}(k)H_0[a\xi] \exp(jkz)}{\xi^2 [(H_0[r\xi])^2 - (H_0[a\xi])^2]} dk \quad (24)$$

$$I_2(z) = 4\epsilon_0 \frac{1}{2\pi} \int_{-\infty}^{\infty} \frac{\tilde{E}_{z1}(k)H_0[r\xi] \exp(jkz)}{\xi^2 [(H_0[r\xi])^2 - (H_0[a\xi])^2]} dk \quad (25)$$

In order to obtain explicit expressions for $I_1(z)$ and $I_2(z)$ the impressed longitudinal electric field sources along the outside of the source cable shield must be determined.

Recall that Z_t is the ratio of the resultant electric field on one side of the shield to the current flowing on the opposite side. Therefore, the mechanism of the surface transfer impedance directly gives rise to an impressed longitudinal electric field along the outside of the shield. For the present case this is given in eq. (1). Upon taking the Fourier transform of (1) we have

$$\tilde{E}_{z1}(k) = 2\pi \frac{1}{k} + \beta Z_t I_s \quad (26)$$

Substituting this expression into eq.'s (24) and (25) and integrating we obtain

$$I_1(z) = -4\epsilon_0 \frac{Z_t I_s H_0[a\xi_2] \exp(-j\beta z)}{2 [(H_0[r\xi_2])^2 - (H_0[a\xi_2])^2]} \quad (27)$$

$$I_2(z) = 4\epsilon_0 \frac{Z_t I_s H_0[r\xi_2] \exp(-j\beta z)}{2 [(H_0[r\xi_2])^2 - (H_0[a\xi_2])^2]} \quad (28)$$

where $\xi_2^2 = k_0^2 - \beta^2$. Eq.'s (27) and (28) are the

expressions for the surface transfer impedance contribution to the external shield currents.

Since the integral equation approach requires an excitation in terms of an impressed longitudinal electric field, and the effect of the transfer admittance is typically modeled using a distributed current source, it is necessary to find an equivalent impressed electric field source to account for the transfer admittance.

To this end, consider the configuration shown in Fig. 2. This consists of a coaxial cable of length L suspended at a height H over an infinite ground plane. The cable height is small compared to a wavelength such that the shield and ground plane constitute a second transmission line. For computational convenience the shield ends are assumed to be terminated to the ground plane in the characteristic impedance of this second transmission line. However, this does not affect the generality of the conclusions obtained from the following discussion.

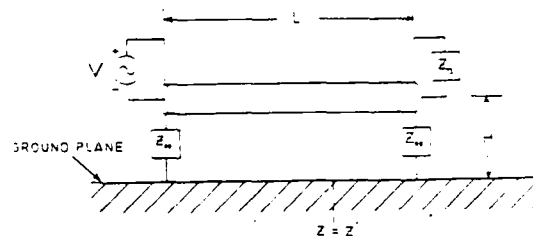


Fig. 2. Theoretical configuration for calculating the equivalent voltage used in determining the V_t contribution to the external shield currents.

The coaxial cable is driven at one end and, through the mechanism of the surface transfer impedance and the transfer admittance, energy is coupled from the coaxial cable into the secondary line. Presently we are only concerned with the transfer admittance contribution.

Initially the coaxial cable is assumed to be perfectly shielded except over a short section of braid centered at $z=z'$. The distributed current source is then well approximated by a delta function source of strength $V_t(z') Y_t \exp(-j\beta z')$. Here a phase factor has been included for future convenience.

The current distribution is calculated using the current source part of eq. (3). Therefore we have

$$I(z) = \frac{V_t Y_t}{2} \exp(-j\beta z') \begin{cases} \exp(jk_0(z' - z)), & z > z' \\ -\exp(jk_0(z - z')), & z < z' \end{cases} \quad (29)$$

The current distribution of eq. (29) has a current flowing in opposite directions away from the source, producing a total current of zero at $z=z'$. We now wish to obtain an equivalent voltage source which will produce this same current distribution. Intuitively, we require a source which is positive in sign at $z=z'+$ and negative at $z=z'-$, but zero at $z=z'$. One function which satisfies these conditions is the

derivative of a delta function.

Consider then a voltage distribution of the form

$$V_s(z) = A\delta'(z-z') / z \quad (30)$$

impressed on the transmission line at $z=z'$ where A is a constant to be determined. Using the voltage source portion of eq. (3), the current distribution is obtained as

$$I(z) = \frac{-A}{2Z_0} jk_0 \begin{cases} -\exp(jk_0(z'-z)), & z > z' \\ \exp(jk_0(z-z')), & z < z' \end{cases} \quad (31)$$

In order for the current distributions of eq. (31) and eq. (29) to be equal we must have

$$A = \frac{-V_s Y_t Z_0}{jk_0} \exp(-j\beta z') \quad (32)$$

Note that for the external transmission line $k_0 = \sqrt{LC_e}$ where C_e is the external capacitance per unit length between the cable shield and the ground plane and L is the per unit length inductance of the shield over the ground plane. Therefore eq. (32) can be written as

$$A = \frac{-V_s Y_t}{j\omega C_e} \exp(-j\beta z') = -V_s S_c \exp(-j\beta z') \quad (33)$$

where C_i is the internal capacitance per unit length inside the cable.

Fourier transforming eq. (30) and using eq. (33) we have

$$V_s(k) = -jkV_s S_c \exp(-j\beta z') \quad (34)$$

Substituting this into eq.'s (24) and (25) and integrating first over z' and then over k , we obtain

$$I_1(z) = 4\omega\epsilon_0 \frac{V_s j\beta C_p H_0 [a\epsilon_2] \exp(-j\beta z)}{\beta^2 [(H_0 [r\epsilon_2])^2 - (H_0 [a\epsilon_2])^2]} \quad (35)$$

$$I_2(z) = -4\omega\epsilon_0 \frac{V_s j\beta C_p H_0 [r\epsilon_2] \exp(-j\beta z)}{\beta^2 [(H_0 [r\epsilon_2])^2 - (H_1 [a\epsilon_2])^2]} \quad (36)$$

Eq.'s (35) and (36) are the transfer admittance contribution to the external shield currents.

5. Relationship Between Transmission Line Theory and the Integral Equation Approach

If the integral equation approach is more general than transmission line theory, then the transmission line results should be contained in the integral equation results. To show that this is indeed the case define two new currents I_d and I_c as follows:

$$I_d = I_2 - I_1, \quad (37)$$

$$I_c = I_2 + I_1, \quad (38)$$

I_d is called the differential mode current and I_c is called the common mode current. The reason for using this nomenclature becomes clear when we solve (37) and (38) for I_1 and I_2 :

$$I_1 = I_c - I_d \quad (39)$$

$$I_2 = I_c + I_d \quad (40)$$

Thus, I_c is the in phase current component on the two cable shields (i.e., in the same direction) and I_d is the 180° out of phase component (i.e., in opposite directions).

Adding eq. (27) to (35) and (28) to (36) and substituting these into eq.'s (39) and (40) we obtain

$$I_d = 2\omega\epsilon_0 S_c \frac{(Z_t - Z_{0s} j\beta C_p) \exp(-j\beta z)}{\beta^2 [H_2 [D\epsilon_2] - H_1 [a\epsilon_2]]} \quad (41)$$

$$I_c = 2\omega\epsilon_0 S_c \frac{(Z_t - Z_{0s} j\beta C_p) \exp(-j\beta z)}{\beta^2 [H_2 [D\epsilon_2] + H_1 [a\epsilon_2]]} \quad (42)$$

Using the small argument approximation for H_0 , recalling the expression for Y_t , and noting that $C_e = 4\omega\epsilon_0 / Z_0$, eq. (41) reduces to

$$I_d(z) = \frac{-I_s}{k_0} \frac{Z_t jk_0}{2 - \beta^2 Z} \left[\frac{Z_t jk_0}{2} - Y_t Z_{0s} j\beta \right] \exp(-j\beta z) \quad (43)$$

Eq. (42) is identically equal to eq. (43), the expression for I_c . Therefore, the transmission line external shield current is just the differential mode current obtained in the integral equation approach.

6. Internally Induced Voltages

Given the induced external current on the receptor cable shield the voltages induced along the inside of the receptor cable can be calculated using transmission line theory. In the present case coupling to the interior of the receptor cable only takes place along the braided portion of length L . Also, since the cable is infinite in length, it is matched on the inside at $z=0$ and $z=L$. Under these conditions the near-end and far-end voltages are given by

$$V(0) = \frac{I_0}{j\beta} (Z_t + j\beta C_p Z_0) \exp(-j\beta 2L) \quad (44)$$

and

$$V(L) = \frac{I_0}{j\beta} (Z_t - j\beta C_p Z_0) \exp(-j\beta L) \quad (45)$$

respectively, where I_0 is the amplitude of the external shield current calculated using either transmission

line theory or the integral equation approach.

Plotted in Fig. 3 is the far-end crosstalk as a function of frequency for separations of 5, 10, 20, and 40 cm. The dashed lines denote transmission line results and the solid lines correspond to the integral equation results. Theoretical values for Z_t and Y_t are used. These can be found in reference [6].

According to transmission line theory the crosstalk increases with frequency at a rate of 20dB/decade. The integral equation result, however, increases at a rate of 20dB/decade only at low frequencies and small separations. When the frequency increases to a point where the separation is greater than about a tenth of a wavelength the crosstalk predicted by the integral equation approach begins to decrease.

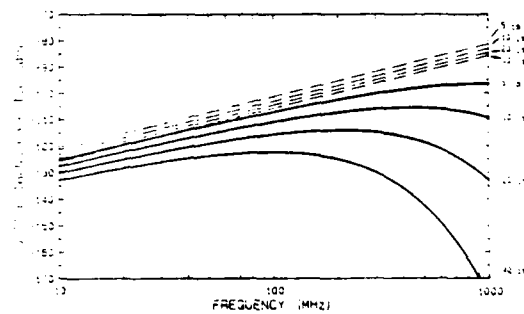


Fig. 3. Far-end crosstalk in the infinite cable case for RG58 coaxial cable. The dashed and solid lines correspond to transmission line theory and the integral equation approach, respectively. The corresponding cable separations are denoted on the right.

In Fig. 4 is shown the far-end crosstalk as a function of separation for frequencies of 10, 100, and 500 MHz. According to transmission line theory the

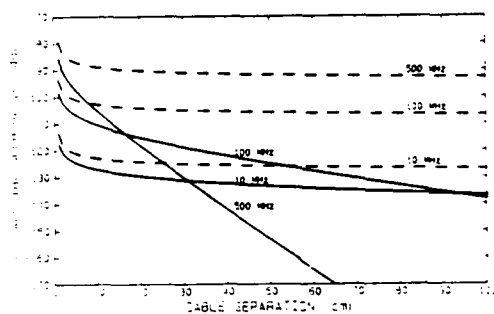


Fig. 4. Far-end voltage transfer ratio as a function of cable separation in the infinite cable case. The dashed and solid lines correspond to transmission line theory and the integral equation approach, respectively. The cable type is RG58 and the interaction length is 1 meter.

crosstalk is greater the higher the frequency. This occurs regardless of separation. The integral equation approach, however, exhibits this behavior only for small separations. At larger separations, according to the integral equation approach, the crosstalk decreases with increasing frequency.

7. Experimental Procedure

In order to verify the theory FEXT measurements were made on an "infinite" cable configuration. The experimental setup is shown in Fig. 5. Infinite cables were simulated using ferrite rings along the cable ends to eliminate end reflections of the external shield currents. By eliminating the end reflections only traveling wave external shield currents are present and therefore the experimental setup approximates the ideal configuration of Fig. 1.

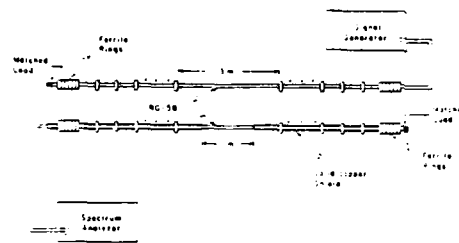


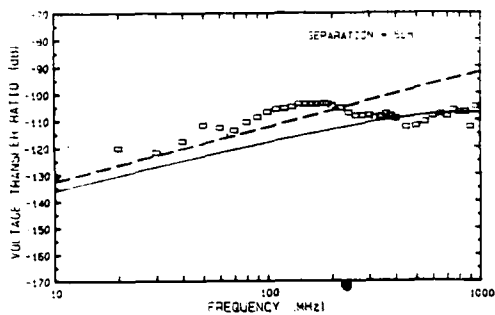
Fig. 5. Experimental setup.

The source cable consisted of a 6m length of RG58/U coax with ferrite rings placed along 1.5m of the cable at each end. The rings were spaced 5 cm apart except at the ends, where six rings were placed close together. The receptor cable consisted of three sections: a 1m length of RG58A/U coax in the middle and a 2.5m solid shielded cable section on each end. Ferrite rings were placed on the solid shielded sections with the same spacing as on the source cable. The source cable was driven at one end with a signal generator and the coupled signal was measured at the opposite end on the receptor cable using a spectrum analyzer. Both cables had matched terminations.

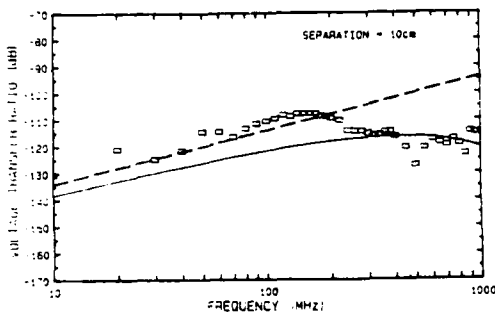
The results of FEXT measurements for separations of 5, 10, and 20 cm are shown in Fig.'s 6a, 6b, and 6c, respectively. Theoretical curves of the integral equation approach and transmission line theory are also plotted. Measured values of Z_t and Y_t were used for the theoretical curves. At the lower frequencies the measured data increases at a rate of 20 dB/decade as predicted by both theories. At the higher frequencies the data tracks very well with the integral equation result but falls off rapidly from the transmission line results.

8. Conclusions

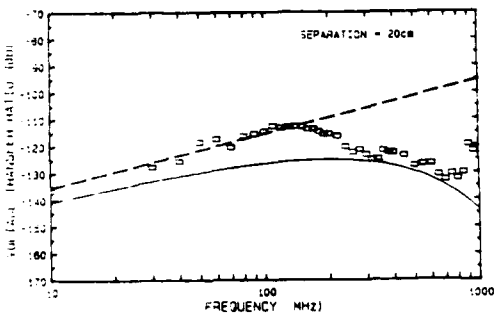
In this paper an integral equation approach has been developed for analyzing coaxial cable crosstalk. The major difference between this new approach and traditional transmission line theory is in the determination of the external shield currents. Inherent in the transmission line theory approach is the assumption that the induced currents on the two cable shields are equal in magnitude and opposite in sign. That is, only the differential mode current is considered. The integral equation approach considers



(a)



(b)



(c)

Fig. 6 Far-end crosstalk in the infinite cable case for RG-58 coaxial cable. The dashed and solid lines correspond to transmission line theory and the integral equation approach, respectively. The rectangles are experimental values. The interaction length is 1m.

both the differential mode and the common mode current. At small separations the differential mode current is dominant and the two theories give comparable results. For large separations, however, the common mode and the differential mode current are

of the same order and both must be included in the analysis.

Although the measured crosstalk at low frequencies is higher than that predicted by both theories, over the whole frequency range the experimental data tracks well with the integral equation approach. In particular, as the separation is increased, the integral equation approach correctly predicts the fall off of the crosstalk at high frequencies.

The infinite cable configuration discussed in this paper was chosen because it gives good physical insight into the coupling mechanisms. Although the results presented here apply to a specific configuration, the general approach can be applied to other configurations as well. In particular, its application to resonant configurations will be discussed in a future publication.

Acknowledgements

Support for this project was provided under contract No. N66604-86-M-G895 by the Office of the Chief of Naval Research/Office of Naval Technology; Submarine Technology Program Element; Program Element Manager is Mr. Gene Remmers, Code 233. Block Program Manager for the Submarine Technology Block Program is Mr. Lincoln Cathers, Code 012.4, of the David Taylor Naval Ship Research & Development Center. Principal Investigator of "The Ships Below-Decks EMC Program" is Mr. David S. Dixon, Naval Underwater Systems Center, Code 3431.

References

- [1] S.A. Schelkunoff and T.M. Oradenko, "Crosstalk Between Coaxial Transmission Lines," Bell Sys. Tech. J., Vol. 16, pp. 144-164, April 1937.
- [2] A.H. Badr, F.A. Benson, and J.E. Sitch, "Interference Between Braided Coaxial Cables," IEE Proc., Vol. 128, Pt. A, No. 5, pp. 347-353, July 1981.
- [3] S. Sali, F.A. Benson, and J.E. Sitch, "General Crosstalk Equations Between Two Braided Coaxial Cables in Free Space," IEE Proc., Vol. 130, Pt. A, No. 6, pp. 306-312, Sept. 1983.
- [4] C.R. Paul, "Transmission-Line Modeling of Shielded Wires for Crosstalk Prediction," IEEE Trans. Electromagn. Compat., vol. EMC-23, No. 4, pp. 345-351.
- [5] A.H. Badr, F.A. Benson, and J.E. Sitch, "Coupling Between Coaxial Cables Over a Ground Plane at Low Frequencies," IEE Proc., vol. 127, Pt. A, No. 8, pp. 549-552, Nov. 1980.
- [6] E.F. Vance, *Coupling to Shielded Cables*, Chap. 3 and 5, John Wiley & Sons, New York, (1978).
- [7] R.W.P. King and Sheila Prasad, *Fundamental Electromagnetic Theory and Applications*, Chap. 3, Prentice-Hall, Englewood Cliffs, New Jersey (1986).

DEVELOPMENT OF MODELS FOR THE SHIELD-GROUND ADAPTER

R.M. Showers and Steven Peters
 Moore School of Electrical Engineering
 University of Pennsylvania
 Philadelphia, PA 19104-6390

Abstract

A theoretical model is presented for an adapter to be used for grounding the external shield of a cable to a plate it penetrates. The model shows good agreement with measurements up to at least 500 MHz.

1. Introduction

The Shield Ground Adapter (SGA) is a device for bypassing undesired induced currents on the outer conductor of a shield or cable to a conducting surface through which it passes.

Figure 1 gives a functional diagram of the configuration. Vertical electric fields intercepted by the cable induce external currents on the shield. We assume the area below the cable penetration is in a perfectly shielded area, i.e., there is no penetration of the area by the external field except at the exposed cable penetration. The energy intercepted is primarily scattered by the part of the cable exposed to the field. The SGA will cause induced current to flow radially from the exposed cable over the upper surface of the conducting plate. Skin depth principles will apply to the current in this surface. At HF almost all current will appear within a fraction of a millimeter of the surface.

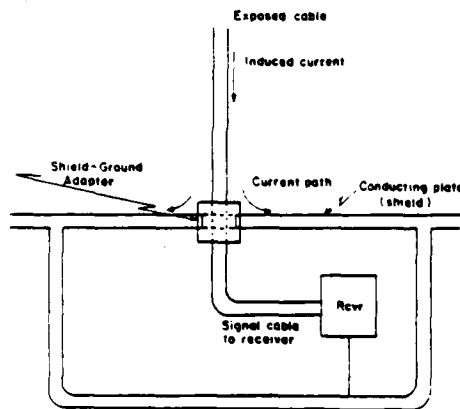


Fig. 1. Functional schematic diagram for shield-ground adapter.

Figure 2 shows an equivalent circuit model of the adapter and connected cables. The parameters Z_s and Z_L represent impedances as seen looking into the cables leading away from the adapter and V_s is an equivalent source voltage. The impedances Z_{su} , Z_{sg} , and Z_{sl} represent an equivalent circuit of the adapter

itself. Z_s and Z_L must be estimated using transmission line theory. If the exposed cable is represented as a vertical antenna above a ground plane, Z_s would be the driving point impedance at the conducting surface, where the cable enters the adapter and V_s the open circuit voltage at this point.

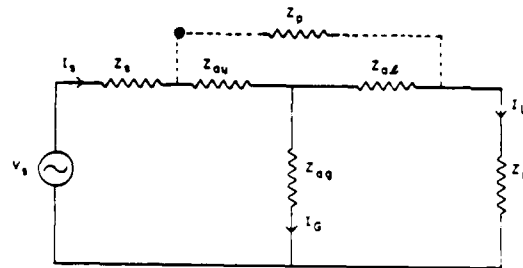


Fig. 2. Equivalent circuit of shield-ground adapter and connected cables.

Z_p represents a possible shunting effect in the SGA itself or in the cable to the shield of which the SGA makes contact. These effects are discussed in detail in par. 11. In the discussion that immediately follows, the possible existence of Z_p is ignored.

2. The Exposed Cable

The exposed cable can exist in either a terminated or unterminated condition, i.e., it can be connected to a separate "ground" return or it can be left open circuited on the mast of the ship. While the method of termination may be quite significant at lower frequencies, at higher frequencies it is less important.

At low frequencies, if the exposed cable "floats" the source impedance Z_s will be a highly capacitive reactance. If it is "grounded" so as to form a loop above deck Z_s will be an inductive reactance. In this case, at sufficiently low frequencies the current induced will be limited by the cable shield resistance. At higher frequencies, the induced currents may be limited by cable inductance. At still higher frequencies, whether the cable is open circuited or short circuited, the induced currents may be quite large due to resonance effects.

3. Measures of Effectiveness

The shielding effectiveness of the SGA is most simply stated in terms of the current bypassed to the conducting plate by the adapter. Ignoring Z_p in Fig. 2, one can calculate the effectiveness to be

$$\frac{I_s}{I_L} = \frac{Z_{sg} + Z_{sl}}{Z_{sg}}$$

In actual use the cable shield on the output side of the SGA is connected to ground, so that at low frequencies Z_L consists of the cable shield resistance and inductance. At higher frequencies, transmission line theory must be applied and measurements of Z_{ag} and Z_{at} may not be easily separated from Z_L . Because of this, measurements may be more meaningful for characterizing the SGA if made with a terminated (e.g. 50 ohm) transmission line structure constituting Z_L . Such measurements can be made at frequencies up to above 1 GHz.

With the 50 ohm termination, the SGA attenuation becomes

$$\frac{I_s}{I_L} = \frac{50}{Z_{ag}} \quad (2)$$

4. Model Impedance Characteristics

The elements Z_{au} , Z_{ag} , and Z_{at} of the SGA itself can be expected to have only resistive components at the lower frequencies of interest. As the frequency increases reactive components will appear. To get orders of magnitude at 1 MHz copper has a surface resistivity of 0.00038 ohms per square and a skin depth of 0.0067 cm or 2.7 mils. For a radial flange with an inner radius of 1/2" and an outer radius of 3/4" the resistance of Z_{ag} would be approximately

$$R = \frac{R_s l}{w} \quad (3)$$

where

R_s is the surface resistivity in ohms per square
 l is the radial length of the flange
 w is the circular length

i.e.,

$$R = \frac{0.00038 \times \frac{1}{8}}{2 \times \frac{1}{2}} = 1.5 \times 10^{-5} = 15 \text{ micro-ohms}$$

The attenuation would then be given by ignoring depth of penetration effect.

$$\frac{I_s}{I_L} = \frac{50}{1.5 \times 10^{-5}} = 33 \times 10^5 = 130.4 \text{ dB} \quad (4)$$

The corresponding transfer impedance would be 36.4 dB (or 130.4 dB 50Ω) with a short-circuited output table of resistance R_L , the attenuation would be

$$\frac{I_s}{I_L} = \frac{R_L}{1.5 \times 10^{-5}} \quad (5)$$

5. Equivalent Circuit

The identification of a more exact equivalent circuit for the SGA requires a careful analysis of current patterns on the structure of the SGA as well as the installation itself. Parameters of the SGA can

be isolated to the greatest extent possible by placing the SGA in a coaxial configuration as shown on Fig. 3. This figure shows 5 transmission lines corresponding to the distances shown as Z_1 , Z_2 , Z_3 , Z_4 , and Z_5 . On the input side line 1 is loaded with lines 2 and 3 in series, and on the output side line 4 is loaded by line 5. The input side is assumed driven on the left-hand side and the output side is terminated on the right-hand side, either in a short circuit or in the characteristic impedance of line 5. The former is perhaps most representative of actual conditions, especially at low frequencies, but the latter condition gives more uniform results for measurement of SGA parameters.

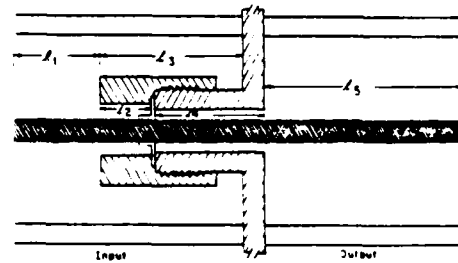


Fig. 3. Model of shield-ground adapter with coaxial configuration.

The coupling between input and output sections is assumed to occur across the flange separating lines 2 and 4. Initially, coupling between lines 3 and 5 is assumed negligible because of the wide thickness of the barrier plate separating them. This assumption may require further consideration depending on the method used to mount the SGA to the barrier plate.

One way of estimating the coupling due to the flange is to use the model shown in Fig. 4 and to calculate the resistance of the flange taking into account the distribution of current density with depth in the flange. The resulting coupling can be expressed in terms of a transfer impedance defined as the ratio of the voltage impressed on the output line to the current in the input line.

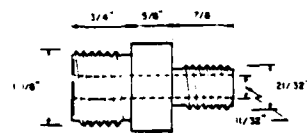
Schelkunoff¹ has calculated the transfer impedance per unit length for a thin walled tube as

$$Z_{12} = \frac{1}{2\pi a \sigma} \frac{(1+j)\sqrt{\frac{2}{\delta}}}{\sinh(\pi a \sqrt{\frac{2}{\delta}})} \text{ ohms meter} \quad (6)$$

where a is the radius of the tube, δ is its thickness, σ is the conductivity and δ is the skin depth. Extending this formula to the disc-shaped flange the mean radius \bar{r} corresponds to a and l corresponds to the length.

The transfer impedance thus becomes

$$Z_{12} = \frac{2\pi \bar{r} l}{2\pi a \sigma l} \frac{(1+j)\sqrt{\frac{2}{\delta}}}{\sinh(\pi a \sqrt{\frac{2}{\delta}})} \text{ ohms} \quad (7)$$



Subhood mounting section of SGA connector (side view)

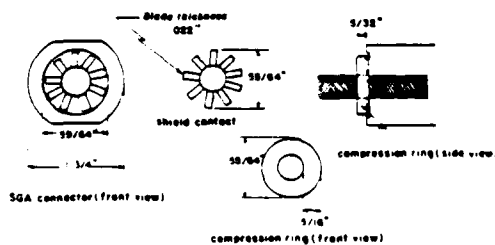


Fig. 4. Internal construction of SGA connector.

Thus the voltage applied across the input to line 4 is $V_{i2}^2 Z_{i2}$, where I_{2R} is the total current at the end of line 2.

Now if $V(0)$ is the line voltage at $z=0^2$, then

$$V(z) = V(0) \frac{Z_1 \cosh \gamma_1 (l-z) + Z_0 \sinh \gamma_1 (l-z)}{Z_1 \cosh \gamma_1 l + Z_0 \sinh \gamma_1 l} \quad (8)$$

and

$$I(z) = \frac{V(0)}{Z_0} \frac{Z_2 \cosh \gamma_2 (l-z) + Z_3 \sinh \gamma_2 (l-z)}{Z_2 \cosh \gamma_2 l + Z_3 \sinh \gamma_2 l} \quad (9)$$

where l is the length of a line of characteristic impedance Z_0 loaded with an impedance Z_1 and propagation constant γ_1 . From (8) and (9) the input impedance Z_{i1} is

$$Z_{i1} = Z_0 \left[\frac{Z_1 \cosh \gamma_1 l + Z_0 \sinh \gamma_1 l}{Z_2 \cosh \gamma_2 l + Z_3 \sinh \gamma_2 l} \right] \quad (10)$$

6. The Input Line

If a line is terminated in a short circuit, its input impedance is given by from Eq. 10 above,

$$Z_{i1} = Z_0 \tanh \gamma_1 l$$

$$\frac{I_{i1}}{V_{i1}} = \frac{I_{2R} \cosh \gamma_2 l + I_{3R} \sinh \gamma_2 l}{V_{i1} \cosh \gamma_1 l + I_{i1} \sinh \gamma_1 l}$$

$\gamma = \alpha + j\beta$ is the propagation constant of the line, and αl is assumed to be small. Therefore, since lines 2 and 3 are always terminated by short circuits

$$Z_{i2} = Z_{02} \tanh \gamma_2 l_2$$

$$Z_{i3} = Z_{03} \tanh \gamma_3 l_3$$

From these equations one can obtain relations between currents at various parts of the configuration. For example, the ratio of the current at the left end of line 2 to that at the right end of line 2 is

$$\frac{I_{2L}}{I_{2R}} = \cosh \gamma_2 l_2 \quad (12)$$

Lines 2 and 3 present a load impedance to line 1 of

$$Z_{L1} = Z_{02} \tanh \gamma_2 l_2 + Z_{03} \tanh \gamma_3 l_3$$

From this impedance the input current to line 1 can be found from 9, i.e.,

$$I_{1L} = \frac{V_{i1}}{Z_{01}} \left[\frac{Z_{01} \cosh \gamma_1 l_1 + Z_{L1} \sinh \gamma_1 l_1}{Z_{L1} \cosh \gamma_1 l_1 + Z_{01} \sinh \gamma_1 l_1} \right] \quad (13)$$

and the ratio of the current on the left end to that on the right end of line 1 is

$$\frac{I_{1L}}{I_{1R}} = \cosh \gamma_1 l_1 + \frac{Z_{L1}}{Z_{01}} \sinh \gamma_1 l_1 \quad (14)$$

7. Output Line

It is common to treat the discontinuity at the point of coupling between lines 4 and 5 as a mismatch in which (using Eq. 10)

$$Z_{i4} = Z_{i5} = Z_{05} \frac{Z_{05} \cosh \gamma_5 l_5 + Z_{04} \sinh \gamma_5 l_5}{Z_{05} \cosh \gamma_5 l_5 + Z_{05} \sinh \gamma_5 l_5} \quad (15)$$

and correspondingly,

$$Z_{i4} = Z_{04} \frac{Z_{04} \cosh \gamma_4 l_4 + Z_{i4} \sinh \gamma_4 l_4}{Z_{04} \cosh \gamma_4 l_4 + Z_{i4} \sinh \gamma_4 l_4} \quad (16)$$

8. Calculation of Shielding Effectiveness

At frequencies high enough for standing waves to exist on the various transmission lines there is possible ambiguity in the measure of effectiveness for the SGA, depending on where the current is measured. To reduce dependence on input and output transmission lines (lines 1 and 5) as much as possible one could use the ratio

$$S.E. = \frac{I_{2L}}{I_{5L}}$$

Now I_{5L} is equal to I_{4R} and $I_{1R} = I_{2L}$. The current I_{4R} is related to the impressed voltage on line 4 by (from 11)

$$I_{4R} = \frac{V_{4L}}{Z_{R4} \cosh \gamma_4 l_4 + Z_{04} \sinh \gamma_4 l_4} \quad (18)$$

From (7) and the discussion following it:

$$V_{4L} = Z_t I_{2R} \quad (19)$$

and from (12) we have

$$I_{2R} = \frac{I_{2L}}{\cosh \gamma_2 l_2} \quad (20)$$

Hence, (17) becomes, using (19) and (20):

$$S.E. = \frac{I_{1R}}{I_{5L}} = \frac{I_{2L}}{I_{4R}} = \frac{\cosh \gamma_2 l_2 I_{2R}}{I_{4R}} = \frac{\cosh \gamma_2 l_2 I_{2L}}{Z_t I_{4R}}$$

Now, from (9)

$$I_{4R} = \frac{V_{4L}}{Z_{04} Z_{15} \cosh \gamma_4 l_4 + Z_{04} \sinh \gamma_4 l_4}$$

or

$$S.E. = \frac{\cosh \gamma_2 l_2}{Z_t} \left(Z_{15} \cosh \gamma_4 l_4 + Z_{04} \sinh \gamma_4 l_4 \right) \quad (21)$$

If l_4 's are small and $Z_{15} = 50 \Omega$

$$S.E. = \frac{50}{Z_t} \quad (22)$$

The shape of the flange is shown on Fig. 4. It is noted that the part between the inner and outer conductors of transmission lines 2 and 4 consists effectively of 9 separate conducting fingers. Calculations of the dc resistance are made as follows:

$$R_{dc}^{finger} = \frac{l}{\sigma w T}$$

For

$$\begin{aligned} l &= 2.8 \times 10^{-7} \text{ m} \\ w &= 2.6 \text{ mm} \\ T &= 2.1 \text{ mm} \end{aligned}$$

one obtains

$$R_{dc}^{finger} = 7.44 \times 10^{-5} \Omega$$

or

$$R_{dc}^{total} = \frac{R_{dc}^{finger}}{9 \text{ fingers}} = 8.26 \times 10^{-6} \Omega \quad (23)$$

9. Mutual Inductance

In addition to coupling from the resistance of the flange of the SGA, there is mutual inductance due to the triangular shaped gaps in the flange. This permits magnetic field leakage to couple energy between transmission lines 2 and 4. This coupling is represented as a mutual inductance M_{24} calculated as follows, by using formulas for circular apertures of the same average radius as the triangular shaped holes⁴:

$$M_{24} = N \frac{\mu_0 m}{4 \pi a^2 Z}$$

for

$$a = \text{avg. radius} = \sqrt{r_1 r_2} = 5.35 \text{ mm}$$

m = magnetic polarizability

N = number of holes

$$m = \frac{4}{3} r^3 \text{ (circular holes)} = 4.57 \times 10^{-10} \text{ for}$$

$$r = 0.7 \text{ mm}$$

$$= \frac{1}{16} (d^2 \text{ rectang. slot}) = 3.19 \times 10^{-10} \text{ for}$$

$$d = 2.1 \text{ mm}, d = 0.38 \text{ mm}$$

Since $N = 9$

$$\text{and } \mu_0 = 4\pi \times 10^{-7}$$

$$M_{24} = m \times 10^{-2} = 3.2 \times 10^{-12}$$

Finally, we have for the transfer impedance

$$Z_t = Z_d + j\omega M_{24}$$

$$Z_d = R_{dc} \frac{(1+j) T/5}{\sinh [(1+j) T/5]} \quad (24)$$

$$s = \frac{1}{\sigma w T}$$

Using these parameter values, the shielding effectiveness characteristic is calculated as shown on Fig. 5. The corresponding value of the transfer impedance for a 50 Ω load is shown as the dotted curve on this figure. On the figure it is noted that the characteristic starts out flat with frequency until the skin depth becomes less than the conductor thickness (at about 100 kHz) with the shielding effectiveness reaching a maximum value at about 500 kHz. Above that frequency the characteristic is dominated by the mutual inductance term, the S.E. decreasing as the frequency increases. This frequency dependent behavior is similar to that which occurs for braided shields on coaxial structures.

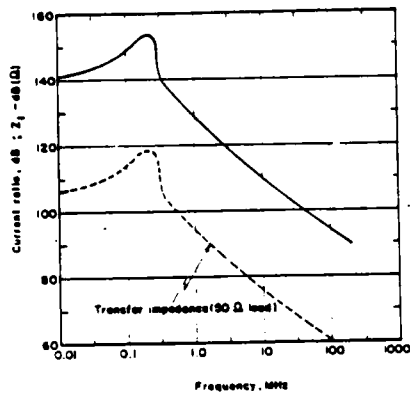


Fig. 5. Shield-ground adapter shielding effectiveness (Iout/Iin) vs. frequency and transfer impedance, Z_t .

10. Correlation with Experimental Data

Experimental data obtained to date on these SGAs show the same trend as in Fig. 5 for frequencies above about 600 kHz. For frequencies below 600 kHz the experimental data are approximately 20 dB higher than that given in Fig. 5. The reason for this appears to be the presence of other coupling mechanisms which are not accounted for in the model discussed to this point.

11. Refining the Equivalent Circuit

As mentioned in the discussion of Fig. 2, a more complex equivalent circuit may be necessary to account for actual experimental behavior of the SGA. The first effect considered is coupling through the center conductor of the shielded cable itself. A second effect is the contact resistance between the cable braid and the flange. A third effect is impedance at the junction of the adapter fitting and the reference or ground plane in which it is mounted.

11.1 Coupling through the Cable

Figure 6 shows the surface transfer impedance for RG-214 cable (which contains a double braid). Assuming the RG-214 cable itself is loaded with 50 Ω, as is the transmission line consisting of the shield and the outer test fixture cylinder, the coupling can be estimated as follows. A current I_s on the shield of the RG-214 will produce for a one meter length of the input cable $Z_{tc} I_s$ volts along the inside of the shield, where Z_{tc} is the surface transfer impedance of the cable itself. This in turn will cause

$\frac{Z_{tc} I_s}{50}$ amperes in the center conductor of the output

cable. This current will produce $\frac{Z_{tc}^2}{50}$ volts in a one meter length of the outer structure. The overall transfer impedance is then

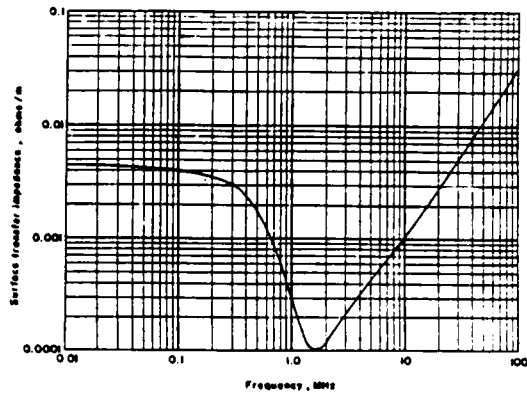


Fig. 6. Frequency response of the surface transfer impedance for RG-214 coaxial cable.

$$\frac{V_o}{I_s} = \frac{Z_{tc}^2}{50} \text{ } \Omega/\text{m}^2$$

This is shown as a function of frequency in Fig. 7. At 10 kHz

$$\frac{V_o}{I_s} \text{ (dB)} = -46 - 46 - 34 = -126 \text{ dB}(\Omega)$$

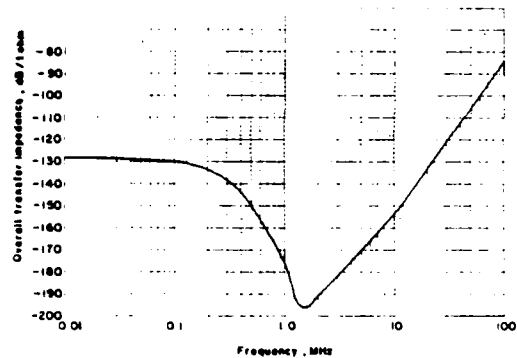


Fig. 7. Overall transfer impedance of RG-214 coaxial cable with a 50 ohm load when fitted with the SGA.

This corresponds with a voltage ratio of -150 dB for a load resistance on transmission line 5 of 50 Ω, when compared with Fig. 5 it is seen that, for input and output lengths of one meter, the cable has a coupling contribution equivalent to that of the SGA. For longer lengths, the cable itself becomes the weakest link in the system, for example, if the length of the cable extends 10 m on either side of the SGA, the coupling by this mechanism increases by 40 dB giving a voltage ratio of -110 dB. For single braid cables the

coupling would be increased further. Tests being conducted presently are with a total cable length of only about 6" (15 cm).

11.2 Flange Contact Resistance

This is the contact resistance of the flange where it is soldered to the cable braid. Normally, this is considered negligible because the skin effect will cause the current to leave the shield and appear on the surface of the flange (with highest current density on the input side of the flange). Since the conducting surface of the cable is a braid, there may be a tendency for some of the input current to follow individual braid wires and not pass to the flange. If the contact resistance is of the order of only tens of microhms, the current would be expected to flow through the contact resistance, rather than be shunted across the flange by capacitive effects. (For example, a capacitance of 50 pF has an impedance of 3000 Ω at 1 MHz.) Accordingly, the transfer impedance between input and output circuits due to such a contact resistance would be equal to the contact resistance.

11.3 Adapter Fitting Ground Plane Junction

Figure 8 is a schematic drawing of the adapter fitted to the ground or reference surface. (For simplicity, only one half of the adapter bisecting plane is shown.) Experimental evidence has shown that the threads holding the several parts together have measurable contact resistance. The threads TH 1 will have little effect on the adapter's

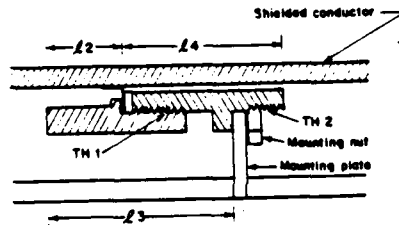


Fig. 8. Detail of Fig. 3 showing threads and contact resistances contributing to transfer impedance.

overall transfer impedance as they add only a very small resistance, say 10^{-5} ohms, to the load on transmission line 3. Compared with the approximately 50 ohm characteristic impedance of transmission line 3, it will have little effect. The resistance of these threads does not directly introduce a voltage into the output circuit. Threads TH2 on the other hand (and the contact resistances between (1) the clamping nut mounted on threads TH 2 and the ground plate, and (2) between the ground plate and the outer test fixture tubes), will directly couple energy from the input of the adapter to its output. For frequencies for which transmission lines 2, 3, and 4 are short compared with a quarter wave length (typically up to 250 MHz or higher), one has the equivalent circuit shown in Fig. 9. From this equivalent circuit one obtains a total transfer impedance Z_T , using Eq. 24 and Fig. 9.

$$Z_T = Z_C + R_{TH} \quad (25)$$

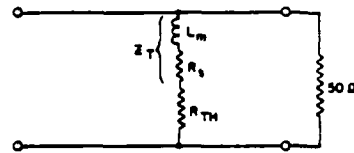


Fig. 9. Equivalent circuit at frequencies less than (typically) 250 MHz showing effect of resistance of threads and contacts. Adapter load resistance, 50 Ω .

For a 50 ohm output cable termination the shielding effectiveness is

$$S.E. = \frac{50}{Z_T} \quad (26)$$

Equations 25 and 26 are plotted in Fig. 10 for values of R_{TH} of 5, 10 and 20 microhms. It is seen that as R_{TH} increases, the variation of the overall transfer impedance with frequency decreases.

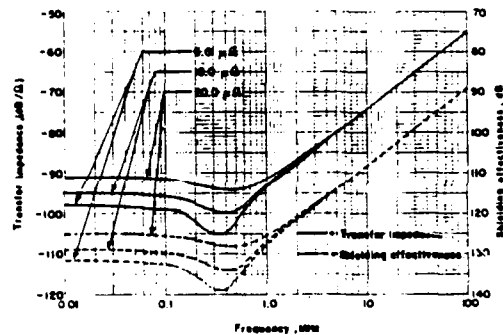


Fig. 10. Frequency response of the shielding effectiveness and total transfer impedance of the SGA for values of thread resistance of 5, 10 and 20 microhms.

12. Conclusions

A fairly exact model for a shield ground adapter contains a term for transfer impedance of the element shorting the cable shield to the body of the connector, plus terms taking account of resistances at threads and contacts of the mounting arrangement. The cable surface transfer impedance places an upper limit on the shielding effectiveness that can be obtained. At frequencies above 250 MHz, transmission line elements must be included in the model.

Acknowledgement

This work was performed under P.O. 8L 4722 for G&H Technology, Camarillo, CA under prime contract N70024-3068-1076. Support for this project was provided by the Office of The Chief of Naval Research/Office of Naval Technology; Submarine Technology Program Element; Program Element Manager is Mr. Gene Remmers, Code 233. Block Program Manager for the Submarine Technology Block Program is Mr. Lincoln Cathers, Code 012.4 of the David Taylor Naval Ship Research & Development Center. Principal Investigator of "The Ships Below-Decks EMC Program" is Mr. David S. Dixon, Naval Underwater Systems Center, New London, CT, Code 3431.

References

- [1] Edward F. Vance, COUPLING TO SHIELDED CABLES, Wiley-Interscience, 1978, p. 113.
- [2] J.G. Brainerd, et. al., ULTRA HIGH FREQUENCY TECHNIQUES, Van Nostrand, 1942.
- [3] Edward F. Vance, COUPLING TO SHIELDED CABLES, Wiley-Interscience, 1978, p. 35.
- [4] Edward F. Vance, "Shielding Effectiveness of Braided-Wire Shields," IEEE Trans. on Electromagnetic Compatibility, Vol. EMC-17, pp. 71-77, May 1975.

INITIAL DISTRIBUTION LIST

	No. of Copies
<u>External</u>	
NAVSEA (SEA-06D, -06D4, -06D443, -06D444, -06DE, -56Z1, -56Z2, -61R4)	8
NAVAIR (AIR-5161F)	
CNO (OP-941FC (Dr. R. Haislmaier))	1
SPAWAR (32DT)	1
OCNR/ONT (Code 233 (G. Remmers), Code 234 (J. Cauffman))	2
DWTNSRDC (Code 012.4 (L. Cathers))	1
UPenn (Dr. R. Showers)	1
Western New England College (J. Masi)	1
G & H Technology, Inc., Camarillo Office	1
Eldyne Inc., New London Office	1
Analysis & Technology, Inc., New London Office	1
DTIC	12
 <u>Internal</u>	
Codes: 10	1
10 (Dr. Kasper)	1
34	1
3491 (Dr. Miller)	1
341	1
342	1
343	1
3431 (EMC Branch, J. Boucher, D. Dixon (3))	5
40	1
41	1
44	1
44 (A. Bruno)	1
0211 (R. Bernier)	1
02151 (New London)	2
02152 (Newport)	1